

Evolution of Elliptical Galaxies at $z \gtrsim 1$ Revealed from a Large, Multicolor Sample of Extremely Red Objects ¹

M. Miyazaki ², K. Shimasaku ^{2,3}, T. Kodama ⁴, S. Okamura ^{2,3}, H. Furusawa ⁵, M. Ouchi ²,
 F. Nakata ⁴, M. Doi ⁶, M. Hamabe ⁷, M. Kimura ⁸, Y. Komiyama ⁵,
 S. Miyazaki ⁵, C. Nagashima ⁹, T. Nagata ⁹, T. Nagayama ⁹, Y. Nakajima ⁹,
 H. Nakaya ⁵, A. J. Pickles ¹⁰, S. Sato ⁹, K. Sekiguchi ⁵, M. Sekiguchi ⁸,
 K. Sugitani ¹¹, T. Takata ⁵, M. Tamura ⁴, M. Yagi ⁴, and N. Yasuda ⁴

shimasaku@astron.s.u-tokyo.ac.jp

ABSTRACT

We study the evolution of elliptical galaxies at $z \gtrsim 1$ on the basis of a sample of 247 Extremely Red Objects (EROs) with $R - K_s \geq 3.35$ (AB) and $K_s \leq 22.1$ (AB) constructed from $BVRi'z'JHK_s$ multicolor data of a 114 arcmin² area in the Subaru/XMM Deep Survey Field taken with the Subaru Telescope and the UH 2.2m Telescope. This is the largest multicolor sample of EROs covering B to

¹Based in part on data collected at Subaru Telescope, which is operated by the National Astronomical Observatory of Japan.

²Department of Astronomy, School of Science, University of Tokyo, Tokyo 113-0033, Japan

³Research Center for the Early Universe, School of Science, University of Tokyo, Tokyo 113-0033, Japan

⁴National Astronomical Observatory of Japan, Mitaka, Tokyo 181-8588, Japan

⁵Subaru Telescope, National Astronomical Observatory of Japan, 650 N. A'ohoku Place, Hilo, HI 96720, USA

⁶Institute of Astronomy, School of Science, University of Tokyo, Mitaka, Tokyo 181-0015, Japan

⁷Department of Mathematical and Physical Sciences, Faculty of Science, Japan Women's University, Tokyo 112-8681, Japan

⁸Institute for Cosmic Ray Research, University of Tokyo, Kashiwa, Chiba 277-8582, Japan

⁹Department of Physics, Nagoya University, Oizu-cho, Chikusa-ku, Nagoya 464-8602, Japan

¹⁰Institute for Astronomy, University of Hawai'i, 640 N. A'ohoku Place, Hilo, HI 96720, USA

¹¹Institute of Natural Sciences, Nagoya City University, Mizuho-ku, Nagoya 467-8501, Japan

K_s bands ever obtained. The threshold of $R - K_s \geq 3.35$ is set to select passively evolving galaxies at $z \geq 0.8$. By fitting template spectra of old ellipticals (OEs) and young, dusty starbursts (DSs) to the multicolor data, we classify EROs into these two classes and estimate their redshifts. In order to express possible star formation superposed on an old stellar population for OEs, the OE templates include combinations of a passively evolving bulge component and a star-forming disk component.

We find that 58% of the EROs in our sample belong to the OE class. These OEs have a wide range of colors at any redshift, suggesting that OEs at $z \geq 0.8$ cannot be described by a single, passive evolution model with a fixed formation redshift (z_F). We also find that 24 % of the OEs are fit by a spectrum having a disk component with the B -band bulge-to-total luminosity ratio of ≤ 0.9 , implying that a significant fraction of OEs at $z \geq 0.8$ have a non-negligible amount of star formation.

A comparison of the observed surface density of OEs with predictions from passive evolution models with $z_F = 5, 3, 2.5$, and 2 shows that the $z_F = 3$ and 2.5 models reproduce the observed counts fairly well while the $z_F = 5$ model and $z_F = 2$ model overpredict and underpredict, respectively, counts at faint magnitudes. In this paper we adopt an $\Omega_0 = 0.3$ and $\lambda_0 = 0.7$ cosmology. We then derive rest-frame B -band luminosity functions (LFs) of OEs in our sample at $z = 1 - 1.5$ and $1.5 - 2.5$. We find that the LF at $z = 1 - 1.5$ roughly agrees with the LF of local ellipticals if a dimming of 1.3 mag from $z = 1.25$ to the present is assumed; this amount of dimming is predicted by a passive evolution with high formation redshifts, $z_F \geq 3$. On the other hand, the amplitude of the LF at $z = 1.5 - 2.5$ is found to be lower than that of the local LF by a factor of ~ 3 over the whole range of magnitude observed when a dimming predicted by the $z_F = 5$ passive evolution model is considered. This deficiency becomes larger if models with lower z_F are adopted, meaning that the matches of the $z_F = 3$ and 2.5 models to the observed number counts are superficial. Taking account of a strong decrease in the number density of morphologically classified early-type galaxies at $z \gtrsim 1.5$ found by several authors, we conclude that the majority of ellipticals seen at present have not established either a red color or a smooth 1/4-law profile before $z \sim 1.5$.

The angular correlation function of OEs shows a strong clustering. The spatial correlation length is estimated to be $r_0 = 11 \pm 1 h^{-1}$ Mpc, which is larger than that for the present-day early-type galaxies of similar luminosities. This suggests that OEs are selectively located in regions which will become present-day clusters or groups of galaxies.

Finally, we examine properties of DSs in our data. The DSs are found to have a wide range of redshifts, with a peak of the distribution at ~ 1.5 , and to have $E(B - V) \sim 0.4 - 1.2$ with a median of $\simeq 0.8$. The dust-corrected SFR values are found to span $10^{1-3} M_{\odot} \text{ yr}^{-1}$. Combined with a strong clustering seen in our DS sample, these high SFR s may suggest that DSs are progenitors of part of the present-day E/S0s.

Subject headings: galaxies: elliptical and lenticular, cD — galaxies: evolution — galaxies: photometry

1. INTRODUCTION

The formation and evolution of early-type galaxies are one of the central issues of modern astronomy. The evolution of early-type galaxies at $z \lesssim 1$ has been relatively well constrained by many observations. Tight color magnitude relations have been found in early-type galaxies, and the evolution of these relations has also been studied up to $z \sim 1$ (e.g., Bower, Lucey, & Ellis 1992; Ellis et al. 1997; Kodama et al. 1998; Stanford, Eisenhardt, & Dickinson 1998). Luminosity functions of red galaxies and morphologically classified early-type galaxies up to $z \sim 1$ do not show clear number evolution but show mild brightening with redshift (Lilly et al. 1995; Brinchmann et al. 1998; Lin et al. 1999; Im et al. 2002). These observations suggest that the evolution of early-type galaxies up to $z \sim 1$ is well approximated by the passive evolution, i.e., a pure luminosity evolution after a starburst at the initial phase of their formation at high redshifts.

On the other hand, recent observations of more distant galaxies have revealed that early-type galaxies at $z \gtrsim 1$ do not appear to obey the passive evolution. Franceschini et al. (1998) have found a trend that the number density of morphologically classified early-type galaxies drops at $z \gtrsim 1.5$. Similar results have been derived by Rodighiero et al. (2001) and by Kajisawa & Yamada (2001). Kodama, Bower, & Bell (1999) and Menanteau et al. (2001) have shown that a significant fraction of early-type galaxies in fields at $z \sim 1$ have colors bluer than predictions from passive evolution models. Early-type galaxies that are blue in the rest-frame UV colors have also been found in clusters at $z > 1$ (e.g., Tanaka et al. 2000; Haines et al. 2001; Nakata et al. 2001).

Extremely Red Objects (hereafter EROs), which are defined as objects having red optical-to-infrared colors such as $R - K \geq 5$ in the Vega-based magnitude system, are a suitable population for studies of elliptical galaxies at $z \gtrsim 1$, since a large fraction of EROs are thought to be passively evolving galaxies at high redshifts. EROs were first discovered by

the K -band surveys by Elston, Rieke, & Rieke (1988, 1989). Since then many authors have detected EROs in near infrared surveys, although definitions of EROs are slightly different among the authors.

EROs are thought to be a mixture of mainly two different populations at $z \gtrsim 1$; passively evolving old elliptical galaxies (hereafter OEs) and dusty starburst galaxies whose UV luminosities are strongly absorbed by internal dust (hereafter DSs). Both populations satisfy color thresholds for EROs, e.g., $R - K \geq 5$ (Vega), if they are located at $z \gtrsim 1$. These two populations can be discriminated by their morphology or locations in color-color spaces. Stiavelli & Treu (2001) have classified 30 EROs on the basis of morphology of HST/NICMOS images, to find about 60% of them are consistent with ellipticals. Similarly, Moriondo, Cimatti, & Daddi (2000) have found the fraction of ellipticals in their ERO sample to be 50 – 80%. Mannucci et al. (2002) have separated the two populations using $R - K$ vs $J - K$ colors and have found that the two populations have similar abundances in their 57 EROs (see also Pozzetti and Mannucci 2000). To summarize, about a half or more of the whole EROs seem to be OEs.

EROs have been used to place constraints on the evolution of elliptical galaxies at $z \gtrsim 1$. Barger et al. (1999) have found in a 61.8 arcmin² area that only a small number of galaxies have colors redder than $I - K = 4$ (Vega), and inferred that only a fraction of the local elliptical galaxies have formed in a single burst at high redshifts. On the other hand, McCracken et al. (2000) have detected about three times more EROs with $I - K \geq 4$ (Vega) in a field of 47.2 arcmin². More recently, Daddi, Cimatti, & Renzini (2000b) have found, on the basis of a survey of a much wider area (~ 850 arcmin²), a good agreement between the observed surface density of EROs and predictions by passive evolution models, emphasizing that surveys of small fields are likely to suffer from field-to-field variations of ERO density, because EROs are strongly clustered (Daddi et al. 2000a).

Since EROs are rare and clustered, wide-field surveys are essential for the studies of statistical properties of OEs like number density. Furthermore, as EROs are a mixture of OE and DS populations, it is also necessary to remove DSs from ERO samples in order to investigate the OE population. Among the previous studies on evolution of elliptical galaxies using EROs, none is based on an OE/DS-separated sample from a wide (~ 100 arcmin²) area survey. We have recently completed an imaging survey of a 114 arcmin² area in the $B, V, R, i', z', J, H, K_s$ bands, and detected 247 EROs with $R - K_s \geq 3.35$ (AB mag). These multicolor data enable us not only to classify the EROs into OEs and DSs by colors but also to estimate their photometric redshifts. In this paper, we study the number density and colors of the OEs in this sample, and give strong constraints on the evolution of elliptical galaxies at $z \gtrsim 1$.

The structure of this paper is as follows. We describe observations and data reduction in §2. The ERO sample is constructed in §3. Classification of EROs into the two populations is performed in §4, and results and discussion are presented in §5. The method of classification is described in Appendix. In §6, we give a brief description on dusty starburst galaxies found in our sample. A summary is given in §7.

In what follows, AB magnitudes are used throughout if otherwise noted. The Vega-based magnitudes are represented by (Vega) when necessary. The scales between the Vega-based magnitudes and the AB magnitudes are given by the following formulae: $K_{s,AB} = K_{s,Vega} + 1.8$ and $(R - K_s)_{AB} = (R - K_s)_{Vega} - 1.6$. Here we assume the zeropoint flux of our “Vega” system K_s to be 6.9×10^{-21} erg s⁻¹ cm⁻² Hz⁻¹. We adopt an $\Omega_0 = 0.3$ and $\lambda_0 = 0.7$ cosmology, and express the Hubble constant as $H_0 = 100h$ km s⁻¹ Mpc⁻¹.

2. OBSERVATIONS, DATA REDUCTION, AND PHOTOMETRY

2.1. Optical Data

We took deep B -, V -, R -, i' -, and z' -band imaging data of a central $30' \times 24'$ area in the Subaru/XMM-Newton Deep Survey Field ($2^h18^m00^s, -5^\circ12'00''$ [J2000]) with the prime focus camera (Suprime-Cam; Miyazaki et al. 2002) mounted on the 8.2m Subaru telescope during the commissioning observing runs on November 24-27, 2000 and October 14, 18, 19 and November 17, 2001. The image scale of Suprime-Cam is 0."202 per pixel. The individual CCD data were reduced and combined using IRAF and the mosaic-CCD data reduction software developed by us (Yagi et al. 2002). The combined images for individual bands were aligned and smoothed with Gaussian kernels to match their seeing sizes. The B , V , i' data and part of the R data (58min), all of which were obtained in 2000, have already been reduced by Ouchi et al. (2001) for studies of Lyman Break Galaxies at $z \sim 4$. Hence, in this study we reduced the z' and newly added R data alone. The final images cover a contiguous 618 arcmin² area with a PSF FWHM of 0."98. Photometric calibrations are made using photometric standard stars given in Landolt (1992) for B , V , R data and spectrophotometric standard stars given in Oke (1990) for i' (SA95-42) and in Bohlin, Colina, & Finley (1995) for z' (GD71). Transformation from Vega-based magnitudes to AB magnitudes is made following Fukugita, Shimasaku, & Ichikawa (1995). The photometric zero points for B , V , and i' data are the same as those adopted in Ouchi et al. (2001). A summary of the optical data is given in Table 1.

2.2. Infrared Data

Wide-field J , H , K_s data were obtained with the University of Hawaii (UH) 2.2m Telescope at Mauna Kea on the nights of August 28 to September 4, 2001. The observations were made using Simultaneous 3-color InfraRed Imager for Unbiased Survey (SIRIUS; Nagayama, Nagashima, Nakajima et al. 2002). SIRIUS is a three-color simultaneous camera employing three 1024×1024 HgCdTe arrays. The field of view at each band is $4.7' \times 4.7'$, with a pixel size of $0.''28$. SIRIUS was developed as an infrared imager for the Nagoya University 1.4m telescope at South African Astronomical Observatory (SAAO), but it can also be mounted on the UH 2.2m Telescope.

Six pointings (133 arcmin^2 in total) were made with SIRIUS in the 618 arcmin^2 region imaged by Suprime-Cam. For each pointing, we obtained 120 dithered exposures, each being 1 minute long. The net exposure times of J , H , and K_s images for a single pointing are thus 120 min each. J data were not successfully acquired for a quarter of the field of view due to a detector problem. The area covered by J is thus 75% of that covered by H and K . Figure 1 shows the regions on the sky of our optical and infrared observations.

The reduction of the J , H , and K_s data are carried out using IRAF. Dome flat-fielding and sky subtraction with a median sky frame are applied. The reduced data are then aligned to the Suprime-Cam optical images. The typical positional accuracy of the J , H , and K_s images relative to the optical ones is estimated to be 0.2 arcsec using common stars. The final image covers a 114 arcmin^2 area for H and K_s and a 77 arcmin^2 area for J , both having a PSF FWHM of $0.''98$, the same value as for the optical images. Photometric calibrations are made using standard stars of Persson et al. (1998), and we do not make any color transformation between their system and the SIRIUS system. A summary of the infrared data is also given in Table 1.

We examine photometric accuracies of our optical + NIR data using stars. We compare colors of stars in our images with those of 175 bright stars in the spectrophotometric atlas by Gunn & Stryker (1983) calculated using our system response functions. We find that for any combination of two colors a systematic deviation of the locus of our stars from that of Gunn & Stryker's in the two-color plane is less than $\simeq 0.05 \text{ mag}$.

2.3. Object Detection and Photometry

Object detection and photometry are made using SExtractor version 2.1.6 (Bertin & Arnouts 1996). The K_s -band image is chosen to detect objects. If more than 5 pixels whose counts are above $2 \sigma_{sky}$ are connected, they are regarded as an object. In total 1308 objects

are detected down to $K_s = 22.1$ mag.

For each object detected in the K_s image, Kron magnitudes are measured for all the bands. Our Kron magnitude, m_K , is defined as $m_K = -2.5 \log L(< 2.5r_K)$, where $L(< 2.5r_K)$ is the luminosity within the circle of radius $2.5r_K$ and r_K is the Kron radius (Kron 1980) in the K_s band. The r_K value for the Kron magnitude is different for different galaxies. The fraction of $L(< 2.5r_K)$ is about $\sim 96\%$ of the the total luminosity for both galaxy and star profiles convolved with Gaussian seeing (Bertin & Arnouts 1996). We apply the Kron radius measured in the K_s image to images in other bands to ensure that the colors are measured within the same aperture for any object.

All magnitudes are corrected for Galactic absorption using Schlegel, Finkbeiner, & Davis (1998), though the amount of absorption is quite small: 0.08 mag for B .

2.4. Star-Galaxy Separation

Star-galaxy separation is made on the basis of $B - i'$ and $B - K_s$ colors and FWHM of objects. Figure 2 plots $B - K_s$ against $B - i'$ for all the objects in the K_s -limited sample (dots), together with 175 stars in Gunn & Stryker’s (1983) spectrophotometric atlas (open triangles). On the basis of this figure, we regard an object as a star and remove it from the sample, if it satisfies simultaneously $B - K_s < 1.583(B - i') - 0.5$ and $\text{FWHM} \leq 1.''2$. The threshold of FWHM is imposed so that clearly non-stellar extended objects are not removed irrespective of their colors. In total 95 objects are regarded as stars and removed.

Large filled circles in Figure 2 denote EROs to be selected by $R - K_s$ color in the next section. The distribution of EROs is well separated from the stellar sequence, and thus it is expected that the ERO sample does not suffer from either the incompleteness due to misidentifying EROs as stars, or the contamination due to misidentifying stars as EROs.

3. THE ERO SAMPLE

We define in this paper EROs as objects whose $R - K_s$ color is equal to or redder than 3.35, or equivalently 4.95 in the Vega-based magnitude. The threshold value corresponds to the apparent color of a passively evolving galaxy at $z = 0.8$ predicted on the basis of Kodama & Arimoto’s (1997; KA97) population synthesis models. In more detail, this model galaxy, being formed at $z = 5$, has the slope of the initial mass function (IMF) of $x = 1.10$, the e -folding star formation timescale of $\tau_{\text{SF}} = 0.1$ Gyr, the e -folding gas infall timescale of $\tau_{\text{infall}} = 0.1$ Gyr, and the age when the galactic wind blows (ie, no star formation occurs after

this) of $t_{\text{GW}} = 0.2$ Gyr. This model reproduces well the average colors of massive elliptical galaxies observed at $z \lesssim 1$ (Kodama et al. 1998).

Figure 3 plots $R - K_s$ as a function of K_s magnitude for all objects except for stars in our K_s sample. The horizontal line denotes our boundary for the ERO selection, and the dotted line corresponds to the 3σ detection limit for R magnitudes. There are 247 objects which satisfy the ERO threshold, $R - K_s \geq 3.35$, down to $K_s = 22.1$ mag. We refer to these objects as the ERO sample.

We estimate the completeness and contamination of our ERO sample as a function of apparent magnitude by Monte Carlo simulations. We generate 2500 objects that mimic the distribution in the $R - K_s$ vs K_s plane of objects with $K_s \leq 22.1$, and distribute them randomly on our original R and K_s images after adding Poisson noises according to their original brightness. We here assume the shapes of generated objects to be Gaussian, with their FWHM values scattered over the range of real objects, $\sim 1'' - 2''$. Then, we run the SExtractor in the same manner as for the original images, detect these simulated objects, and measure their brightness, if detected. We define here the completeness of the ERO sample as the number of the simulated objects which again pass the color threshold divided by all the original objects which passed the threshold. The contamination of the sample is defined as the number ratio of the objects that did not pass the threshold in the original data but satisfy the threshold in the simulated data, due to photometric noises, divided by the number of all the original objects which passed the threshold. The differential completeness is found to drop to 50% at $K_s \simeq 21.6$ mag. The ‘cumulative’ completeness down to $K_s = 22.1$, which is the completeness weighted by the number of the detected objects, is estimated to be 60%. The contamination is found to be lower than 10% over the whole magnitude range.

Figure 4 shows cumulative number counts of EROs in our sample after correction for completeness and contamination, together with those taken from the literature. The filled circles denote our results. The open circles, open triangle, star, filled triangle, and cross are the counts taken from Daddi et al. (2000a; based on an area of 701 arcmin²), Thompson et al. (1999; 154 arcmin²), Cimatti et al. (2002; 52 arcmin²), Scodreggio & Silva (2000; 43 arcmin²), and Cohen et al. (1999; 14.6 arcmin²), respectively. We find from this figure that our counts match reasonably well with Daddi et al.’s (2000a) over $20 \lesssim K_s \lesssim 21$ and with Thompson et al.’s (1999) and Cimatti et al.’s (2002) at $K_s = 21.8$. Cohen et al. have given a bit lower count at $K_s = 21.8$, but the difference is within Poisson errors. Scodreggio & Silva (2000) have obtained a significantly smaller count, which might be due to field-to-field variations.

4. CLASSIFICATION OF EROs USING THEIR MULTICOLORS

In this section, we classify our EROs into two classes, passively evolving old ellipticals (OEs) and dusty starbursts (DSs), using $BVRi'z'JHK_s$ colors.

4.1. Brief Summary of the Method

The method of our classification is a variant of the photometric redshift technique. We use model spectra computed on the basis of stellar population synthesis models by KA97. A major difference from the ordinary photometric redshift technique (e.g., Furusawa et al. 2000) is that the model spectra we use are restricted to those appropriate to OEs and DSs. The model spectra of OEs include those with some ongoing star formation as well as those of passively evolving population.

First, a set of model spectra for OEs and DSs over the redshift range of $0 \leq z \leq 4$ are generated. Effect of dust extinction is taken into account. Next, the spectra are convolved with the system response functions to give the magnitudes to be observed in the bands used in this study. In this process, the effect of absorption due to intergalactic HI gas is taken into account. Then, observed magnitudes of an ERO are compared with model magnitudes and the χ^2 value is computed for all the models. Finally, for each ERO, we identify the model which gives the smallest χ^2 value and assign the class of that spectrum to the ERO.

Out of the 247 EROs in our sample, 143 are classified as OEs while 104 are classified as DSs. Our method gives the estimated photometric redshift and some parameters useful to investigate systematic properties of EROs in addition to their classifications. Details of the model spectra and the technique are given in Appendix.

4.2. Comparison with Classification Based on $J - K_s$ vs $R - K_s$ Colors

Pozzetti & Mannucci (2000) have introduced a method to classify EROs into OEs and DSs on the basis of their locations in the $J - K$ vs $R - K$ plane. This simple method makes use of a characteristic difference in the spectra of OEs and DSs located at $1 \leq z \leq 2$; OEs have a sharp spectral break around 4000\AA while DSs' spectra are smoother, giving DSs' $J - K$ colors redder than OEs'. This method has been recently applied to 57 bright EROs by Mannucci et al. (2002) using $J - K_s$ vs $R - K_s$.

As a check of the validity of our spectrum fitting method, we apply this $J - K_s$ vs $R - K_s$ method to our EROs. Figure 5 shows the result. Filled and open symbols indicate

OEs and DSs, respectively, classified by our spectrum fitting method. The solid line denotes the boundary for the two classes based on $J - K_s$ vs $R - K_s$ colors; objects redder in $J - K_s$ than this line are classified as DSs. According to Mannucci et al. (2002), their method is valid only for EROs satisfying $R - K_s > 3.68$ (horizontal line in Figure 5) and $1 \leq z \leq 2$, and cannot estimate redshift.

The agreement between the two methods is found to be satisfactory. Among the EROs with $R - K_s > 3.68$, about 66 % of the EROs classified as OEs by our method are also regarded as OEs by the $J - K_s$ vs $R - K_s$ method. Similarly, 30 out of the 39 EROs which are classified as DSs by our method are located at the right-hand side of the solid line. There are 23 EROs (with $R - K_s > 3.68$) which are classified as OEs by our method but are located at the right-hand side of the solid line. However, 61 % of them are at either $z < 1$ or $z > 2$, in which the $J - K_s$ vs $R - K_s$ method does not return a reliable answer. In other words, if we restrict ourselves to those objects located at $1 \leq z \leq 2$, 82% of OEs and 77% of DSs classified by our method are found to be classified as OEs and DSs, respectively, by the $J - K_s$ vs $R - K_s$ method.

Our spectrum fitting method uses eight bandpasses from B to K_s . This wide-range and fine sampling of spectra enable us to classify securely EROs over a wider range of redshift than covered by the simple $J - K_s$ vs $R - K_s$ method. In addition, our method estimates photometric redshifts, which are essential for our studies of the evolution of OEs.

4.3. Results of Classification

4.3.1. Relative Mix of OEs and DSs

Out of the 247 EROs in our sample, 143 and 104 are classified as OEs and DSs, respectively, by our spectrum fitting method. The fraction of OEs is thus 58 %. No significant difference is found in the distribution of χ^2 values between the OE and DS populations. Mannucci et al. (2002) have classified 57 EROs down to $K' = 21.8$ by the $J - K$ vs $R - K$ method and found the fraction of OEs over the sum of OEs and DSs to be $21/42 = 50\%$. Cimatti et al. (2002) have taken spectra of 45 EROs with $K_s < 21$, identified about 70% of them with OEs and DSs, and found that the relative fraction of OEs is $\simeq 50\%$. These two estimates, both are based on spectra of EROs, are consistent with our result.

EROs have also been classified morphologically. Stiavelli & Treu (2001) have detected 30 faint EROs using $R - H_{160}$ color in an area imaged with HST/NICMOS. They have visually inspected HST/NICMOS images, to find that about 60% of the 30 EROs belong to elliptical or S0 galaxies. Moriondo et al. (2000) have made a quantitative study of the morphology

of 41 EROs found in images from the HST public archive. They have performed a fit of a generalized exponential profile ($I \propto \exp((R/R_e)^n)$; Sèrsic 1982) to the images, and found that 50 – 80% of the 41 EROs are elliptical-like objects. Vanzella et al. (2001) have reported on the basis of a small sample of EROs in the Hubble Deep Field South that roughly a half of the EROs for which visual classification is successfully made look like elliptical galaxies.

Although morphology and spectrum are independent properties, a rough agreement on morphological and spectrum-based classifications has been reported (e.g., Vanzella et al. 2001). In other words, EROs which have morphological appearance of an elliptical galaxy tend to have a spectrum similar to those of passively evolving galaxies.

4.3.2. Redshift Distributions

We plot in Figure 6 the redshift distribution of OEs (panel [a]) and DSs ([b]) in our sample. The redshift distribution of OEs in our sample has a peak at $z \sim 1$, with a tail toward higher redshifts. The majority of OEs are, however, located at $z < 2$; only 14 % of the total OEs have $z > 2$. It is worth noting that the distribution of our OEs has a sharp cut at $z = 0.8$. We have defined the threshold for EROs, $R - K_s \geq 3.35$, in order to select $z \geq 0.8$ objects. The sharp cut at $z = 0.8$ suggests that the redshift estimation by the spectrum fitting method is reasonable.

The peak of the redshift distribution of DSs in our sample is at $z \sim 1.5$, somewhat higher than the OEs'. Unlike the distribution of OEs, a tail is seen at $z < 0.8$; this is probably because the adopted threshold ($R - K_s \geq 3.35$) is based on passively evolving populations.

Cimatti et al. (2002) have derived the redshift distribution of 14 OEs and 15 DSs for $K_s < 21$ from a spectroscopic survey of EROs with $R - K_s \geq 5$ (Vega). The completeness of their spectroscopic identification is 67%. To compare their results with ours, we plot in Figure 7 the redshift distribution of our 117 EROs brighter than $K_s = 21$ together with Cimatti et al.'s ¹². Although relatively poor statistics of Cimatti et al.'s data do not allow a detailed comparison, a broad agreement is found in the redshift distribution between Cimatti et al.'s and our data for both OEs and DSs. The median redshift of our sample is slightly higher than that of Cimatti et al.'s for both OEs and DSs. This may be partly due to the incompleteness of Cimatti et al.'s spectroscopy, since they claim that due to the noise at

¹²Cimatti et al. present only the redshift distribution from a deeper ($K_s < 21.8$) spectroscopic survey. However, the cumulative completeness of this deeper survey is only 44% and so the number of OEs and DSs identified at $21 < K_s < 21.8$ is only one and three, respectively. Hence, we assume here that the redshift distribution given in Cimatti et al. is actually close to that for $K_s < 21$ objects.

$\lambda > 9000\text{\AA}$, spectroscopic identification was difficult for OEs at $z > 1.3$ and DSs at $z > 1.5$.

4.3.3. Bulge-to-Total Luminosity Ratios

Table 2 shows the distribution of B -band bulge-to-total luminosity ratio B/T for 143 OEs in our sample. All the OEs are found to have $B/T \geq 0.6$, among which 76 % have $B/T > 0.9$. The high average value of B/T suggests that OEs in our sample are progenitors of the present-day elliptical galaxies. On the other hand, the fraction of pure bulges with $B/T = 1$ is not large ($24/143 = 17\%$) (Inclusion of objects with $B/T \geq 0.99$ increases the fraction to 34 %). These results indicate that the majority of the OEs selected in this study have a small but non-negligible amount of star forming component superposed on a dominant old population.

5. RESULTS AND DISCUSSION

5.1. Number Counts

The cumulative number counts, $n(m)$, for OEs in our sample after the completeness and contamination corrections are plotted in Figure 8. The slope of the counts is approximated as $n(m) \propto 10^{0.4 \times m}$ over $K_s = 21 - 22$, and no clear flattening is seen in the magnitude range observed. The surface density of OEs with $K_s < 21$ is estimated to be $0.84 \pm 0.10 \text{ arcmin}^{-2}$. It is apparently a bit larger than Cimatti et al.’s (2002) estimation for OEs, $0.27 - 0.55 \text{ arcmin}^{-2}$, which has not been corrected for completeness. We compare the observed $n(m)$ of OEs with predictions by pure luminosity evolution models of elliptical galaxies.

5.1.1. Prediction by Pure Luminosity Evolution Models

We compute the number counts on the basis of the pure luminosity evolution (PLE) model by KA97 described in §3, i.e., the model with $x = 1.10$, $\tau_{\text{SF}} = 0.1 \text{ Gyr}$, $\tau_{\text{infall}} = 0.1 \text{ Gyr}$, $t_{\text{GW}} = 0.2 \text{ Gyr}$. We examine four values for the formation redshift z_F : $z_F = 5, 3, 2.5$, and 2.

The cumulative surface number density n down to apparent K_s magnitude m is computed as:

$$n = \int_{z_{\min}(z_F)}^{z_{\max}(z_F)} dz \int_{-\infty}^{M_f(z_F, m)} dM \phi(M) \frac{dV(z)}{dz}, \quad (1)$$

where, z_{\min} and z_{\max} are the minimum and maximum redshifts at which the apparent color of the model galaxy satisfies the threshold for EROs, i.e., $R - K_s \geq 3.35$, M_f is the absolute K_s magnitude corresponding to m , $\phi(M)$ is the K_s -band luminosity function (LF) at $z = 0$, and $\frac{dV(z)}{dz}$ is the differential comoving volume. M_f is defined as $M_f = m - (m - M) - K(z) - E(z_F, z)$, where $(m - M)$ is the luminosity distance to an object at z (distance modulus) and $K(z)$ and $E(z)$ are the K and E corrections. Note that z_{\max} , z_{\min} , and M_f are dependent on z_F .

No local K_s -band LF of pure elliptical galaxies is available in the literature. Accordingly, we adopt the B -band LF for elliptical galaxies in the local universe derived by Marzke et al. (1994), which are characterized by the Schechter parameters, $\alpha = -0.85$, $M_B^* = -19.37 - 5 \log h$ (we adopt $B_{AB} = B - 0.14$ following Fukugita et al. 1995), and $\phi^* = 0.0015 h^3 \text{ Mpc}^{-3}$. We convert M_B^* to $M_{K_s}^*$ using $M_{K_s} = M_B - 2.23$ while other parameters are unchanged.

There are a few other sources of the local B -band LF for E/S0 galaxies. Folkes et al. (1999) have obtained, using the 2dF Galaxy Redshift Survey data, $\alpha = -0.74 \pm 0.11$ and $M_B^* = -19.75 \pm 0.09 - 5 \log h$ for local E/S0 galaxies; Marzke et al. (1998) have obtained $\alpha = -1.00 \pm 0.09$ and $M_B^* = -19.51_{-0.11}^{+0.10} - 5 \log h$ for E/S0 galaxies in the Second Southern Sky Redshift Survey data; Kochanek et al. (2001) have derived $\alpha = -0.92 \pm 0.10$ and $M_{K_s}^* = -23.53 - 5 \log h$ (Vega) for E/S0 galaxies in the 2MASS galaxy data. Accordingly, expected uncertainties in α and $M_{K_s}^*$ would be ~ 0.2 and ~ 0.3 , respectively. There are few measurements of ϕ^* for ellipticals alone, but uncertainties in ϕ^* could be as large as a factor of two, because the ϕ^* values derived for E/S0s vary by the same amount (Marzke et al. 1998; Folkes et al. 1999; Kochanek et al. 2001).

5.1.2. Comparison between Observations and Models

Predicted counts are plotted in Figure 8 by a thick solid line ($z_F = 5$), thin solid line (3), dotted line (2.5), and dashed line (2). From a comparison of these predictions with the observed counts, we find that the $z_F = 3$ and 2.5 models match the observed counts fairly well. We assign large weights in the comparison on faint counts with small errors. The $z_F = 5$ model is found to predict the steepest slope of $n(m)$, and largely overshoot the observed counts at faint magnitudes although it predicts correct numbers at bright magnitudes. On the other hand, the $z_F = 2$ model underpredicts counts at faint magnitudes while it tends to produce a bit more galaxies than observed at bright magnitudes. The $z_F = 5$ and 2 models cannot be made consistent with the observation even if possible uncertainties in the local LF are taken into account.

This comparison shows that the range of z_F for which models are consistent with the observed counts is rather limited, i.e., too large and too small z_F values are not favored. It should, however, be noted that the moderate matches of the $z_F = 3$ and 2.5 models to the observed counts do not necessarily mean that OEs obey these models at any redshifts. We will discuss this in the next subsection on the basis of the luminosity function.

Daddi et al. (2000b) have compared surface densities of EROs at $K_s < 21$ selected by $R - K_s$ colors from an area of 850 arcmin² with predictions of passive evolution models, to find a good agreement between the observed surface densities of EROs and those predicted by passive evolution models of $z_F \gtrsim 2.5$. They have not classified EROs into OEs and DSs, but they claim that their results do not change significantly if the fraction of DSs in their sample is less than 30%. In this sense, their results appear to be roughly consistent with ours since the fraction of DSs in our sample, $\simeq 40\%$, is close to 30%.

5.2. Luminosity Functions

We construct the rest-frame B -band LF for OEs in our sample for two redshift bins, $1 \leq z \leq 1.5$ and $1.5 \leq z \leq 2.5$, using the simple $1/V_{\max}$ method. We do not derive LFs at $z > 2.5$ because the OEs in this range are too few. For each OE, the rest-frame B magnitude is computed from the best-fit spectrum.

Figure 9 plots the LFs derived in this way (filled circles with error bars). The solid lines in Figure 9 denote the local B -band luminosity function for ellipticals (Marzke et al. 1994) adopted in §5.1 to predict number counts.

A comparison of the LF derived for the range $z = 1 - 1.5$ with the local measurement finds that while the number density of fainter ($M \gtrsim -19$) OEs at $z = 1 - 1.5$ is comparable to that of the local ellipticals, OEs with $M \lesssim -20$ are much more numerous than in the local universe. Roughly speaking, the LF at $z = 1 - 1.5$ can be fit by the local LF if a dimming of M^* by ~ 1.3 is assumed from $z = 1.25$ to the present epoch. As we see later, this amount of dimming is predicted by the PLE model with $z_F \geq 3$. Similarly, the number density of $z = 1.5 - 2.5$ OEs with $M \lesssim -21$ is found to be much higher than that observed in the local universe. However, unlike the LF at $z = 1 - 1.5$, it is difficult to fit the LF at $z = 1.5 - 2.5$ to the local LF by a shift of M^* alone, because the amplitude of the $z = 1.5 - 2.5$ LF is lower than that of the local LF.

The open circles indicate predictions at $z = 0$ which are calculated by dimming the observed LFs at $z = 1 - 1.5$ (panel [a]) and at $z = 1.5 - 2.5$ (panel [b]) to the present epoch on the basis of the passive evolution model with $z_F = 5$ adopted in §5.1. Similarly,

the open triangles and stars are predictions from the $z_F = 3$ and 2.5 models, respectively. If all ellipticals seen at present obey the passive evolution of, say, $z_F = 5$, then in both panels of Figure 9 the open circles should be on the solid line. In panel (a), the open circles and open triangles match the local LF over almost the whole magnitude range. Taking a smaller value for z_F makes the amount of dimming larger, and thus the LFs evolved to $z = 0$ will become fainter than that of the observed local LF. For instance, the dimming predicted by the $z_F = 2.5$ model appears to be too large by ~ 0.5 mag.

In Figure 9 (b), the difference between the observed local LF and the prediction from the $z = 1.5 - 2.5$ LF is found to be very large for all the three models. Even for the $z_F = 5$ model, which predicts the smallest amount of dimming among the three, the amplitude of the predicted LF is lower than that of the observed local LF by a factor of ~ 3 or so at any magnitudes. If the $z_F = 3$ and 2.5 models are taken, discrepancies at bright magnitudes become quite large; basically no galaxies brighter than -20 mag are predicted by these models. This result means that the fraction of the progenitors of the present-day ellipticals which have obeyed passive evolution at $z > 1.5$ is significantly low. We have found in §5.1 that the $z_F = 2.5$ and 3 models match the observed number counts of OEs. The discrepancies found in the LF at $z = 1.5 - 2.5$ implies that the matches seen in the number counts are superficial. Simply speaking, the number density of OEs predicted by these models is biased towards $z > 1.5$ while the total number of OEs integrated over redshift by these models roughly matches the observed counts.

We have not derived LFs for $z > 2.5$, but a rough estimate shows that the number of observed OEs is much smaller than the prediction of the $z_F = 5$ model. Note that models with $z_F \leq 3$ predict no 'OEs' at $z > 2.5$ since galaxies obeying these models do not satisfy $R - K_s \geq 3.35$ at beyond $z = 2.5$.

5.3. Colors

Figure 10 plots observed $R - K_s$ color as a function of redshift for OEs in our sample. The four solid lines indicate predictions by passive evolution models with $z_F = 20, 5, 3$, and 2. It is found that the number of OEs having colors clearly redder than the prediction by the $z_F = 5$ model is very small. The observed OEs have a wide range of color at any redshift, meaning that the OEs cannot be reproduced by a single, passive evolution model of a specific z_F .

Figure 11 plots $R - K_s$ against $B - R$ for OEs at $z = 1 - 1.5$. The four lines in panel (a) indicate evolutionary tracks from $z = 1.5$ to 1 of passive evolution models with $z_F = 5, 3, 2.5$,

and 2. The majority of the OEs are found to be located outside the region between the $z_F = 5$ and 2 tracks. This suggests that most of the OEs do not have a color consistent with passive evolution models of $z_F \geq 2$. Panel (b) of Figure 11 plots the same data as for panel (a), but the four lines indicate colors from $z = 1.5$ to 1 of a passively evolving bulge of $z_F = 5$ on which a disk component is superposed with the rest-frame B/T ratio of 1 (i.e., pure bulge), 0.99, 0.9, and 0.8. For the data, symbols are changed according to B/T of the best-fit spectrum; open circles for $B/T = 1$, open triangles for $0.99 \leq B/T < 1$, filled circles for $0.9 \leq B/T < 0.99$, crosses for $0.8 \leq B/T < 0.9$, and stars for $B/T < 0.8$. It is found that OEs with lower B/T have bluer $B - R$ color, with $R - K$ color almost unchanged. It is also found that the majority of the OEs fall between the $B/T = 1$ and 0.8 lines. We do not intend to say that most OEs are on evolutionary tracks of a bulge + disk galaxy of $z_F = 5$, because the ages of the best-fit spectra span over a wide range. The point here is that the observed OEs are expressed by bulge + disk models much better than by pure bulges of passive evolution of different ages. This implies that the majority of the OEs in our sample have non-negligible star formation. If we calculate the star formation rate from the best-fit spectrum, we obtain $0.9h^{-2}M_\odot \text{ yr}^{-1}$ for an OE with $K_s = 21$ and $B/T = 0.9$ at $z = 1.25$.

5.4. Clustering

We examine clustering of OEs in our sample. We derive the angular two-point correlation function, $\omega(\theta)$, using the estimator defined by Landy & Szalay (1993), $\omega_{obs}(\theta) = [DD(\theta) - 2DR(\theta) + RR(\theta)]/RR(\theta)$, where $DD(\theta)$, $DR(\theta)$, and $RR(\theta)$ are numbers of galaxy-galaxy, galaxy-random, and random-random pairs normalized by the total number of pairs in each of the three samples. The real correlation function $\omega(\theta)$ is offset by the integral constant (IC : Groth & Peebles 1977); $\omega(\theta) = \omega_{obs}(\theta) + IC$. The value of IC/A_ω in our sample is calculated to be 0.0124, where A_ω is the amplitude of the true angular correlation function at $1''$ (see below). The resulting angular correlation function is plotted in Figure 12 after application of IC . This figure shows that OEs are clearly clustered on the sky. The amplitude of the angular correlation function increases with decreasing θ , and takes $\gtrsim 1$ at $\theta \lesssim 10''$.

We fit a power law, $\omega(\theta) = A_\omega(\theta^{-0.8} - IC)$, to the data points over the range of $3'' \leq \theta \leq 150''$, to find $A_\omega = 6.1 \pm 0.9 \text{ arcsec}^{0.8}$, or equivalently $(8.7 \pm 1.3)10^{-3} \text{ degree}^{0.8}$. This best-fit power-law is shown by a solid line in Figure 12. The power law with an index of -0.8 is found to approximate the data well.

Several papers have measured A_ω of EROs, but all of them are not for the OE population but for the ERO population as a whole. One of the measurements is given in Daddi et al.

(2000b), who select 281 EROs of $R - K_s \geq 5$ (Vega) down to $K_s = 19.2$ (Vega) in a 447.5 arcmin^2 area and find $A_\omega = (13 \pm 1.5)10^{-3} \text{ degree}^{0.8}$. Their selection threshold for EROs is the same as in this paper, $R - K_s \geq 3.35$ (AB). In order to compare with their result, we measure A_ω for all EROs with $K_s \leq 21$ (corresponding to $K_s \leq 19.2$ in the Vega system) in our sample. We find $A_\omega = (11 \pm 2)10^{-3} \text{ degree}^{0.8}$, in good agreement with Daddi et al.'s measurement.

Using the Limber transformation (e.g., Peebles 1980, Efstathiou et al. 1991) and adopting the distribution of photometric redshifts of our OEs, we estimate from A_ω the spatial correlation length r_0 for OEs to be $11 \pm 1 h^{-1} \text{ Mpc}$, where we assume no evolution in comoving space¹³.

Norberg et al. (2002) have measured r_0 for early-type galaxies with $M_B = -19.5$ - -20.5 and $M_B = -21$ - -22 in the local universe to be $\approx 6 h^{-1} \text{ Mpc}$ and $\approx 10 h^{-1} \text{ Mpc}$, respectively. Guzzo et al. (1997) have obtained $r_0 = 8.35_{-0.76}^{+0.75} h^{-1} \text{ Mpc}$ for early-type galaxies with $M_B \geq -19.5$ in the Pisces-Perseus supercluster region. Willmer, da Costa, & Pellegrini (1998) have obtained $r_0 = 5.7 \pm 0.8 h^{-1} \text{ Mpc}$ for early-type galaxies with $M_B \leq -19.5$ in field regions of the local universe. Since the typical luminosity of OEs in our sample is $M_B \sim -20$, the clustering of the OEs in our sample is found to be stronger than (or at least as strong as) those of the present-day early-type galaxies with similar luminosities. This may imply that OEs found at $z > 0.8$ are selectively located in regions which will become clusters or groups of galaxies, where most of the present-day early-type galaxies are found.

Our measurement of r_0 for OEs is consistent with that for the OE population at $z \sim 1$ estimated by Daddi et al. (2002), $r_0 \simeq 5.5 - 16 h^{-1} \text{ Mpc}$, based on a small ($N = 15$) but spectroscopically classified sample of OEs. Our measurement is also similar to those for the ERO population as a whole; McCarthy et al. (2001) have selected red ($I - H \geq 3$ in Vega) galaxies in the Las Campanas Infrared Survey and have estimated r_0 of these galaxies to be $\approx 9 - 10 h^{-1} \text{ Mpc}$ at $z \simeq 1$ based on photometric redshifts. Daddi et al. (2001) have obtained $r_0 = 12 \pm 3 h^{-1} \text{ Mpc}$ for EROs with $R - K_s \geq 5$ (Vega) brighter than $K_s = 19.2$ (Vega) assuming that the redshift distribution for EROs is described by a passive evolution model.

Kauffmann et al. (1999) have calculated r_0 of early-type galaxies for $z = 0 - 2.5$ in a Λ Cold Dark Matter model. They have found that r_0 remains almost constant over this

¹³The redshift distribution of OEs has a long high-redshift tail, which may be partly due to errors in photometric redshifts. However, OEs contained in the tail do not have a large contribution to the estimation of r_0 . Indeed, the r_0 value does not change significantly even if we restrict the redshift range to $z = 0.8 - 1.6$, in which 73% of the all OEs are included.

redshift range, $r_0 \approx 7h^{-1}$ Mpc. Although this value is apparently smaller than that found in this study, their selection criteria for early-type galaxies are different from ours. Thus, a detailed comparison requires corrections for these differences, which is beyond the scope of this paper.

5.5. Implications for the Evolution of Ellipticals at $z > 1$

We have found that there exists a population of galaxies (which we call OEs) at $z > 0.8$ whose red $R - K_s$ colors are consistent with predictions of passive evolution models for elliptical galaxies. The strong clustering ($r_0 \sim 10h^{-1}$ Mpc) found for these OE galaxies supports the assumption that they are high-redshift counterparts of the present-day elliptical galaxies. The spatial distribution of OEs appears to be strongly biased against the distribution of dark matter, since r_0 of the dark matter, which is a decreasing function of redshift, should be much smaller than $\sim 10h^{-1}$ Mpc at $z > 0.8$.

We have found that the spread in color of our OEs is considerably large at any redshift; only a small fraction of OEs are redder than predictions of a pure passive evolution model with $z_F = 5$. This implies that ellipticals at $z > 0.8$ are heterogeneous in terms of the stellar population. In other words, colors of OEs at $z > 0.8$ cannot be reproduced by any single passive evolution model with a fixed z_F . Similar results have been obtained on colors of morphologically selected E/S0s at high redshifts on the basis of small samples from deep but narrow field surveys (e.g., Franceschini et al. 1998; Kodama et al. 1999; Rodighiero et al. 2001). It is also found that $R - K_s$ vs $B - R$ colors of the OEs in our sample are reproduced much better by bulge + disk spectra than by spectra of simple passively evolving bulges, suggesting the presence of a non-negligible star formation activity.

Many authors have claimed a possible decrease in the number density of red galaxies at $z \gtrsim 1$ on the basis of observed surface densities on the sky. For example, Barger et al. (1999) have found in a 61.8 arcmin^2 area to a depth equivalent to $K = 20.1$ (Vega) that only a small population of galaxies have colors redder than $I - K = 4$ (Vega), the color expected for an evolved elliptical galaxy at $z > 1$ (See also McCracken et al. 2000). In this study, we have constructed LFs of OEs to locate the era when the number density of OEs changed and to discuss the number evolution of ellipticals. We have found that the spatial number density of OEs at $z \geq 1.5$ is lower than that of the present-day ellipticals by a factor of ~ 3 (or more) if a dimming of brightness due to passive evolution is taken into account, while the LF of OEs at $z = 1 - 1.5$ matches the local LF of ellipticals if a dimming of 1.3 mag from $z = 1.25$ to the present epoch (the amount of dimming expected for the passive evolution model of $z_F \geq 3$) is assumed.

Our finding on the number evolution for OEs is in parallel with the result obtained by Rodighiero et al. (2001) for morphologically selected E/S0s. Rodighiero et al. (2001) have examined the distribution of (photometric) redshifts for 69 morphologically selected E/S0 galaxies at $K \leq 20.15$ (Vega), among which 38 are at $z > 0.8$, in a total of 11 arcmin^2 area of the HDFN, HDFS, and HDFS/NICMOS. They have found that massive E/S0s tend to disappear from flux-limited samples at $z > 1.4$ (see also Franceschini et al. 1998, Nakata et al. 1999). They have reported that the number of E/S0s detected at $z > 1.5$ is about five times lower than predictions from passive evolution models with $z_F \geq 3$, though it is based on poor statistics (they detected only two galaxies at $z > 1.5$).

These findings collectively suggest that a significant fraction of ellipticals seen at present do not have counterparts at $z \gtrsim 1.5$ in terms of either old stellar population or morphology. We discuss two possibilities which could explain the lack of $z > 1.5$ ellipticals. One is that most ellipticals obey pure luminosity evolution (i.e., no merging) even at these redshifts but that residual star formation superposed on old populations is so strong that they drop out of our color selection for EROs; galaxies with non-negligible star formation are likely to have morphologies significantly different from smooth $1/4$ -law profiles. Indeed, the number of OEs in our sample which are fit by a spectrum of pure passive evolution (i.e., bulge) is very limited, and about 24 % of our OEs are fit by bulge + disk models with $B/T \leq 0.9$. Our threshold $R - K_s = 3.35$ selects galaxies with $B/T \gtrsim 0.8$ at $z = 2$ ($z_F = 5$). Thus, if ellipticals at $z = 2$ have star formation equivalent to $B/T < 0.8$, they will not enter our sample. Note that at $z = 1.25$ the $R - K_s = 3.35$ threshold corresponds to $B/T \gtrsim 0.7$, i.e., the minimum value of B/T passing the threshold increases with redshift. This effect may also contribute to the observed decrease in the number density of OEs from $z = 1 - 1.5$ to $z = 1.5 - 2.5$, but we expect that this effect is relatively small as long as the distribution of B/T for OEs does not change significantly from $z = 1 - 1.5$ to $z = 1.5 - 2.5$, since the fraction of OEs with $B/T \leq 0.8$ is only 12% at $z = 1 - 1.5$. Thus, if we want to attribute the decrease in number density of OEs at $z \geq 1.5$ to residual star formation, we must assume that majority of OEs seen at $z = 1 - 1.5$ had B/T smaller than 0.8 at $z \geq 1.5$.

The other possibility is that the present-day ellipticals have been formed from smaller fragmentary galaxies whose morphologies are not necessarily elliptical. Interestingly, Rodighiero et al. (2000) have found the lack of massive, late-type galaxies at $z > 1.4$ in their sample from the HDFN. Galaxies of any morphological types might have been significantly less massive (i.e., fainter) at $z > 1.5$ than predicted from pure luminosity evolution models. We cannot prove or disprove this possibility using our data, but an interesting trend is noted that bright (≤ -20) OEs predicted at $z = 0$ from the $z = 1.5 - 2.5$ LF using the $z_F = 3$ and 2.5 models is much less numerous than the observed local ellipticals with the same luminosity.

We are planning to estimate photometric redshifts for all galaxies in our K_s -limited sample, to derive color-dependent LFs for them. These LFs will give us strong constraints on the number and luminosity evolutions of galaxy population as a whole with high statistical significance.

6. PROPERTIES OF DUSTY STARBURST GALAXIES

In this section, we briefly summarize the properties of the dusty starburst galaxies found in our data. Out of the 247 EROs in our K_s -limited sample, 104 are found to be DSs according to the spectrum fitting.

As seen in §4, the DSs are distributed over a wide range of redshift, though their abundance relative to OEs becomes lower at $z \gtrsim 2$. A small fraction of them are located at $z < 0.8$.

Figure 13 shows the distribution of $E(B - V)$ for DSs in our sample. The DSs are found to have $E(B - V) \sim 0.4 - 1.2$, with a median value of $\simeq 0.8$. This corresponds to $A_V \simeq 2.5$ mag. The $E(B - V)$ distribution of our DSs is in good agreement with that of Cimatti et al.’s (2002). They have found that the average spectrum of DSs for which they made spectroscopy is fit by a local starburst galaxy with $E(B - V) \sim 0.8$. They have also found that the global shape of the continuum and the average $R - K_s$ color of their DSs can be reproduced by synthetic spectra of star forming galaxies of $x = 1.35$ with $0.6 < E(B - V) < 1.1$ (they have also adopted Calzetti’s [1997] extinction law).

We estimate the star formation rate of DSs in our sample using the luminosity at 2800\AA , L_{2800} , adopting the formula given in Madau, Pozzetti, & Dickinson (1998): $SFR[M_\odot \text{ yr}^{-1}] = L_{2800}[\text{erg s}^{-1}\text{Hz}^{-1}]/(7.9 \times 10^{27})$. We find that the dust-uncorrected SFR spans over $10^{-1} - 10^1 M_\odot \text{ yr}^{-1}$, with a median of $1.2 M_\odot \text{ yr}^{-1}$. If we correct for the dust extinction, the median value increases by two orders of magnitude, which is close to those expected for initial starburst phases of elliptical galaxies in passive evolution models. If such high star formation rates last for longer than 10^8 yr or so, these DSs will be recognized as elliptical galaxies in late epochs, and thus part of the ellipticals seen at present could be descendants of these DSs. This may be able to partly account for the observed lack of OEs at high redshift in comparison with the present-day ellipticals.

Finally, we derive the angular correlation function for DSs in the same manner as for OEs. The result is plotted in Figure 14. The amplitude of angular clustering of DSs is found to be similar to that of OEs at $\theta \gtrsim 20''$, but is much lower at smaller scales. A fit of $\omega(\theta) = A_\omega(\theta^{-0.8} - IC)$ to the data points over $20'' \leq \theta \leq 150''$ gives $A_\omega = 7.1 \pm 1.8$,

corresponding to $r_0 = 12 \pm 2h^{-1}$ Mpc. If taken at face value, this r_0 value is very similar to that for OEs.

If the clustering of DSs is really as strong as that of OEs, this would suggest that, similar to OEs, DSs are also formed in high density peaks of the dark matter fluctuations which will become present-day clusters or groups. This appears to support the hypothesis shown above that DSs are progenitors of part of the present day E/S0s. Daddi et al. (2002) have reported that r_0 of DSs at $z \sim 1$ is less than $\sim 2.5h^{-1}$ Mpc, which is apparently inconsistent with our measurement. However, their estimation is derived from only 18 DSs found in 50 arcmin². On the other hand, their classification is based on spectral features of objects, a more direct indicator than we use in this study. Our DS sample could suffer from a non-negligible contamination by OEs due to mis-classification. In addition, Figure 14 shows that the clustering of DSs on $\lesssim 10''$ may be much weaker than an extrapolation of the best-fit $A_\omega\theta^{-0.8}$ determined at $20'' \leq \theta \leq 150''$. An accurate measurement on small scales using a larger sample may reduce A_ω and thus r_0 significantly.

7. SUMMARY

In order to study properties of elliptical galaxies at $z > 0.8$, we have constructed a large sample of Extremely Red Objects (EROs) from $BVRi'z'JHK_s$ multicolor data of a 114 arcmin² area in the Subaru/XMM Deep Survey Field taken with the Subaru Telescope (B to z') and the UH 2.2m Telescope (JHK_s). We have detected 247 EROs with $R - K_s \geq 3.35$ down to $K_s = 22.1$ in the data. This is the largest multicolor sample of EROs covering B to K_s bands ever obtained.

By fitting template spectra of old ellipticals (OEs) and young, dusty starbursts (DSs) at $z = 0 - 4$ to the multicolor data, we have classified the EROs into these two classes and estimated their redshifts. In order to express modest star formation superposed on old stellar population, we include in the OE templates a wide range of combination of an old population (bulge component) and a young population. We have compared our spectrum fitting method with a simple classification method based on $J - K_s$ vs $R - K_s$ colors, which was introduced by Pozzetti & Mannucci (2000), and found a good agreement between the two in the redshift range where the $J - K_s$ vs $R - K_s$ method is valid ($1 \leq z \leq 2$). We have also shown by Monte Carlo simulations that our method works successfully over $0 < z < 4$.

We have found that 143 (58%) of the EROs in our sample belong to the OE class. The redshift distribution of these OEs has a peak at $z \sim 1$ and a sharp cutoff at $z = 0.8$. The surface density and the redshift distribution of OEs in our sample are broadly consistent with

those given by previous authors. Among the OEs, 24 % are fit by a spectrum composed of bulge and disk components with the B -band bulge-to-total luminosity ratio of ≤ 0.9 . It is also found that the OEs have a wide range of colors at any redshift. These findings suggest not only that OEs cannot be reproduced by a single, passive evolution model with a fixed z_F but also that a significant fraction of OEs at $z \geq 0.8$ have a non-negligible amount of star formation.

A comparison of the observed (cumulative) surface density of OEs with predictions from passive evolution models with $z_F = 5, 3, 2.5$, and 2 shows that the $z_F = 3$ and 2.5 models reproduce fairly well the observed counts while the $z_F = 5$ model and $z_F = 2$ model overpredict and underpredict, respectively, counts at faint magnitudes. In order to see more clearly in what range of redshift elliptical galaxies obey passive evolution, we have derived rest-frame B -band luminosity functions (LFs) of OEs at $z = 1 - 1.5$ and $1.5 - 2.5$ separately. We have found that while the LF at $z = 1 - 1.5$ agrees with the local LF of ellipticals if a dimming of 1.3 mag from $z = 1.25$ to the present epoch is assumed, the amplitude of the LF at $z = 1.5 - 2.5$ is lower than that of the local LF by a factor of ~ 3 over the whole range of magnitude observed, meaning that a strong number evolution has occurred at $1.5 \leq z \leq 2.5$. Therefore, the matches of the $z_F = 3$ and 2.5 models to the observed number counts are superficial. Previous authors have found a strong decrease in the number density of morphologically classified early-type galaxies at $z \gtrsim 1.5$. Thus, the majority of ellipticals seen at present appear not to have established the two main features of ellipticals before $z \sim 1.5$, i.e., a red color and a smooth 1/4-law profile.

We have found that the angular correlation function of OEs shows a strong clustering, with $A_w = 6.1 \pm 0.9 \text{ arcsec}^{0.8}$. We have estimated the spatial correlation length for OEs to be $r_0 = 11 \pm 1 h^{-1} \text{ Mpc}$, which is larger than that for the present-day early-type galaxies of similar luminosities. This suggests that OEs are selectively located in regions which will become present-day clusters or groups of galaxies.

Finally, we have examined properties of the 104 DSs in our data. We have found that the DSs have a wide range of redshifts, with a peak of the distribution at $z \sim 1.5$, and $E(B - V) \sim 0.4 - 1.2$ with a median of $\simeq 0.8$. These redshift and $E(B - V)$ distributions are consistent with previous estimates. The dust-corrected SFR values are found to span $10^{1-3} M_\odot \text{ yr}^{-1}$. These high SFR s and a strong clustering seen in our DS sample may suggest that DSs are progenitors of part of the present-day E/S0s.

We would like to thank the Subaru Telescope staff for their invaluable help in commissioning the Suprime-Cam that makes these difficult observations possible. The SIRIUS project was initiated and supported by Nagoya University, National Astronomical Observa-

tory of Japan, and University of Tokyo under a financial support of Grant-in-Aid for Scientific Research on Priority Area (A) No. 10147207 of the Ministry of Education, Culture, Sports, Science, and Technology of Japan. H. Furusawa, C. Nagashima, T. Nagayama, Y. Nakajima, F. Nakata, and M. Ouchi acknowledge support from the Japan Society for the Promotion of Science (JSPS) through JSPS Research Fellowships for Young Scientists.

A. Method of Classification of EROs

The method of our classification is a variant of the photometric redshift technique. We use stellar population synthesis models by KA97 to make model spectra. KA97 include the chemical evolution of gas and stellar populations. KA97 models have been successfully used to obtain photometric redshifts of the Hubble Deep Field North galaxies (Furusawa et al. 2000; see also Kodama et al. 1999 for an application to low-redshifts).

In the present analysis, we use only a limited number of models which are appropriate for EROs. The model spectra for OEs contain not only spectra of passively evolving populations (i.e., bulge component) but also combined spectra of a bulge component and a disk component (see below) with various bulge-to-total luminosity ratios in the B band, B/T , as shown in Table 3. The reason for adding models with a disk component is to express a star formation which may have occurred in some OEs at high redshifts. For bulges, we adopt $x = 1.10$, $\tau_{\text{SF}} = 0.1\text{Gyr}$, $\tau_{\text{infall}} = 0.1\text{Gyr}$, and $t_{\text{GW}} = 0.2\text{Gyr}$, which are known to reproduce the average color of massive ellipticals in clusters of galaxies (Kodama et al. 1998). For disks, we adopt $x = 1.35$, $\tau_{\text{SF}} = 5\text{Gyr}$, $\tau_{\text{infall}} = 5\text{Gyr}$, and $t_{\text{GW}} = 20\text{Gyr}$ (this means that the galactic wind does not blow by the present-day), which are close to the values estimated for the disk of our Galaxy. We make composite spectra by combining a disk component and a bulge component with the same age to give 18 combinations of different B/T . The range of ages for OE models is set to $1 \leq \text{age (Gyr)} \leq 15$. We adopt very small intervals of B/T at $B/T \geq 0.9$ (see Table 3) in order to completely cover the region in color-color spaces occupied by the observed EROs with a sufficiently small grid. Note that adding a small amount of disk component makes colors of the composite spectrum in short wavelengths, such as $B - R$, drastically blue.

The model spectra for DSs are generated by adding dust extinction to young disk spectra whose parameters are the same as for disks used for OEs (Table 3). However, the maximum age is set to $\leq 1.585\text{ Gyr}$. The range of dust extinction is set to $0 \leq E(B - V) \leq 1.5$ with an interval of $E(B - V)$ of 0.05. We adopt the extinction curve given in Calzetti (1997).

We redshift these model spectra from $z = 0$ to 4 with an interval of 0.05, to obtain a

full set of model spectra for classification of EROs. For each spectrum, we take account of the effect of absorption due to the intergalactic HI gas, following the prescription by Madau (1995); this effect is important only for galaxies at $z \gtrsim 4$. Finally, we convolve each redshifted model spectrum by the system response functions, and obtain a set of ‘model fluxes’ from B to K_s .

For each ERO, we compare the convolved model flux T_i with the observed flux F_i in the i -th bandpass and calculate χ^2 as:

$$\chi^2 = \sum_i^{N_{band}} \frac{(F_i - \alpha T_i)^2}{\sigma_i^2}, \quad (\text{A1})$$

where N_{band} is the number of bands used for the observation and σ_i is an observational error in the i -th band. For a given set of T_i , the value of α which minimizes χ^2 is calculated as:

$$\begin{aligned} \frac{\partial}{\partial \alpha} \chi^2 &= \frac{\partial}{\partial \alpha} \sum_i^{N_{band}} \frac{(F_i - \alpha T_i)^2}{\sigma_i^2} = 0, \\ \alpha &= \frac{\sum_i^{N_{band}} \frac{F_i T_i}{\sigma_i^2}}{\sum_i^{N_{band}} \frac{T_i^2}{\sigma_i^2}}. \end{aligned} \quad (\text{A2})$$

Then, we find the best-fit spectrum which gives ‘the minimum reduced χ^2 ’ out of all the model spectra, and the class and the redshift of the best-fit spectrum are adopted as those of the ERO. At the same time, the best-fit $E(B - V)$ value and the age are derived.

To check the reliability of this method, we carry out Monte Carlo simulations. We randomly select 530 galaxies from the set of model spectra over $z = 0 - 4$, add to them a 10% noise (in each bandpass), which is close to the typical photometric errors for our EROs, and fit the template model spectra to them in the same manner as for the observed EROs. As we mention in the main text, all OEs in our data have $B/T \geq 0.6$. Thus, in order to examine uncertainties in redshift estimates for OEs, we compare in Figure 15 (a) the redshifts of input spectra with the estimated redshifts for OEs whose input $B/T \geq 0.6$. We find that objects with $|z(\text{output}) - z(\text{input})| > 0.5$ are very few, and that the rms scatter around the equality is 0.14 even when no object is clipped. The success rate of classification is found to be high; the fraction of input OEs with $B/T \geq 0.6$ which are correctly classified as OEs with $B/T \geq 0.6$ by the fit is 92%. For the reader’s reference, Figure 15 (b) compares the redshifts of input spectra with the estimated redshifts for the all (530) galaxies. A tight correlation is found between the input and output redshifts, although there are a small fraction of galaxies with a catastrophic error in redshift estimate; the rms scatter around the equality is 0.14 if galaxies with $|z(\text{output}) - z(\text{input})| > 0.5$ are removed.

About 25 % of the EROs in our sample do not have J data. To examine effects of not using J flux on the fit, we make similar Monte Carlo simulations without using J flux. We find that the performances of classification and redshift estimation do not change significantly.

REFERENCES

- Barger, A. J., Cowie, L. L., Trentham, N., Fulton, E., Hu, E. M., Songaila, A., & Hall, D. 1999, *AJ*, 117, 102
- Bertin, E. & Arnouts, S. 1996, *A&AS*, 117, 393
- Bohlin, R.C., Colina, L., & Finley, D. S. 1995, *AJ*, 110, 1316
- Bower, R. G., Lucey, J. R., & Ellis, R. S. 1992, *MNRAS*, 254, 601
- Brinchmann, J. et al. 1998, *ApJ*, 499, 112
- Calzetti, D. 1997, *AJ*, 113, 162
- Cimatti, A. et al. 2002, *A&A*, 381, L68
- Cohen, J. G., Blandford, R., Hogg, D. W., Pahre, M. A., & Shopbell, P. L. 1999, *ApJ*, 512, 30
- Daddi, E., Broadhurst, T., Zamorani, G., Cimatti, A., Röttgering, H., & Renzini, A. 2001, *A&A*, 376, 825
- Daddi, E. et al. 2000a, *A&A*, 361, 535
- Daddi, E. et al. 2002, *A&A*, 384, L1
- Daddi, E., Cimatti, A., & Renzini, A. 2000b, *A&A*, 362, L45
- Efstathiou, G., Bernstein, G., Tyson, J. A., Katz, N., & Guhathakurta, P. 1991, *ApJ*, 380, L47
- Ellis, R. S., Smail, I., Dressler, A., Couch, W. J., Oemler, A., Jr, Butcher H., & Sharples, R. M. 1997, *ApJ*, 483, 582
- Elston, R., Rieke, G. H., & Rieke, M. J. 1988, *ApJ*, 331, L77
- Elston, R., Rieke, M. J., & Rieke, G. H. 1989, *ApJ*, 341, 80

- Franceschini, A., Silva, L., Fasano, G., Granato, L., Bressan, A., Arnouts, S., Danese, L. 1998, *ApJ*, 506, 600
- Folkes, S. et al. 1999, *MNRAS*, 308, 459
- Fukugita, M., Shimasaku, K., & Ichikawa, T. 1995, *PASP*, 107, 945
- Furusawa, H., Shimasaku, K., Doi, M., & Okamura, S. 2000, *ApJ*, 534, 624
- Groth, E. J. & Peebles, P. J. E. 1977, *ApJ*, 217, 385
- Gunn, G. E. & Stryker, L. L. 1983, *ApJS*, 52, 121
- Guzzo, L. Strauss, M. A., Fisher, K. B., Giovanelli, R., & Haynes, M. P. 1997, *ApJ*, 489, 37
- Haines, C. P., Clowes, R. G., Campusano, L. E., & Adamson, A. J. 2001, *MNRAS*, 323, 688
- Im, M. et al. 2002, *ApJ*, 571, 136
- Kajisawa, M. & Yamada, T. 2001, *PASJ*, 53, 833
- Kauffmann, G., Colberg, J. M., Diaferio, A., & White, S. D. M. 1999, *MNRAS*, 307, 529
- Kochanek, C. S. et al. 2001, *ApJ*, 560, 566
- Kodama, T. & Arimoto, N. 1997, *A&A*, 320, 41
- Kodama, T., Arimoto, N., Barger A. J., Aragón-Salamanca, A. 1998, *A&A*, 334, 99
- Kodama, T., Bower, R. G., & Bell, E. F. 1999, *MNRAS*, 306, 561
- Kron, R. G. 1980, *ApJS*, 43, 305
- Landolt, A. U. 1992, *AJ*, 104, 340
- Landy, S. D. & Szalay, A. S. 1993, *ApJ*, 412, 64
- Lilly, S. J., Tresse, L., Hammer, F., Crampton, D., & Le Fevre, O. 1995, *ApJ*, 455, 108
- Lin, H. et al. 1999, *ApJ*, 518, 533
- Madau, P. 1995, *ApJ*, 441, 18
- Madau, P., Pozzetti, L., & Dickinson, M. 1998, *ApJ*, 498, 106
- Mannucci, F. et al. 2002, *MNRAS*, 329, L57

- Marzke, R. O., da Costa, L. N., Pellegrini, P. S., Willmer, C. N. A., & Geller, M. J. 1998, *ApJ*, 503, 617
- Marzke, R. O., Geller, M. J., Huchra, J. P. & Corwin, H. G. Jr. 1994, *AJ*, 108, 437
- McCarthy, P. J. et al. 2001, *ApJ*, 560, L131
- McCracken, H. J., Metcalfe, N., Shanks, T., Campos, A., Gardner, J. P., & Fong, R. 2000, *MNRAS*, 311, 707
- Menanteau, F., Abraham, R. G., & Ellis, R. S., 2001, *MNRAS*, 322, 1
- Miyazaki, S. et al. 2002, submitted to *PASJ*
- Moriondo, G., Cimatti, A., & Daddi, E. 2000, *A&A*, 364, 26
- Nagayama, T. et al. 2002, *SPIE*, 4841, in press
- Nakata, F. et al. 2001, *PASJ*, 53, 1139
- Nakata, F. et al. 1999, *MNRAS*, 309, L25
- Norberg, P. et al. 2002, *MNRAS*, 332, 827
- Oke, J. B. 1990, *AJ*, 99, 1621
- Ouchi, M. et al., 2001, *ApJ*, 558, L83
- Peebles, P. J. E. 1980, *The Large-Scale Structure of the Universe* (Princeton: Princeton Univ. Press)
- Persson, S. E., Murphy, D. C., Krzeminiski, W., Roth, M., & Rieke, M. J. 1998, *AJ*, 116, 2475
- Pozzetti, L. & Mannucci, F. 2000, *MNRAS*, 317, L17
- Rodighiero, G., Franceschini, A., Fasano, G. 2001, *MNRAS*, 324, 491
- Rodighiero, G., Granato, G. L., Franceschini, A., Fasano, G., & Silva, L. 2000, *A&A*, 364, 517
- Schlegel, D. J., Finkbeiner, D. P., & Davis, M. 1998, *ApJ*, 500, 525
- Scodeggio, M. & Silva, D. R. 2000, *A&A*, 359, 953
- Sèrsic, J. L. 1982, *Extragalactic Astronomy*. Reidel, Dordrecht

- Stanford, S. A., Eisenhardt, P. R. M., & Dickinson, M. 1998, *ApJ*, 492, 461
- Stiavelli, M. & Treu, T. 2001, in *Galaxy Disks and Disk Galaxies*, ASP Conference Series Vol. 230, p.603.
- Tanaka, I., Yamada, T., Aragn-Salamanca, A., Kodama, T., Miyaji, T., Ohta, K., & Arimoto, N. 2000, *ApJ*, 528, 123
- Thompson, D. et al. 1999, *ApJ*, 523, 100
- Vanzella, E. et al. 2001, *AJ*, 122, 2190
- Willmer, C. N. A., da Costa, L. N., & Pellegrini, P. S. 1998, *AJ*, 115, 869
- Yagi, M., Kashikawa, N., Sekiguchi, M., Doi, M., Yasuda, N., Shimasaku, K., & Okamura, S. 2002, *AJ*, 123, 66

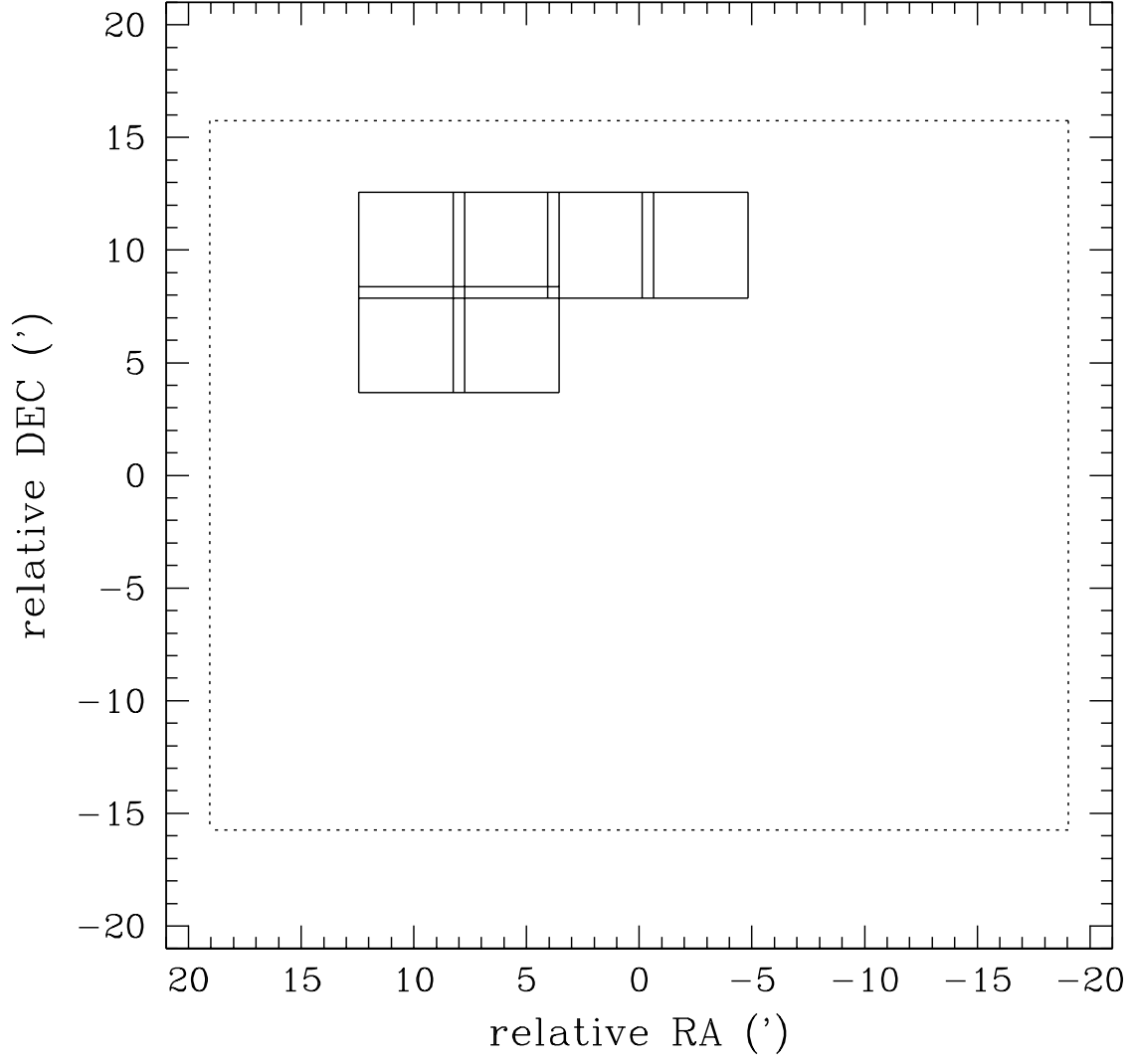


Fig. 1.— Part of the Subaru/XMM-Newton Deep Survey Field. The field observed by Suprime-Cam (B, V, R, i', z') is outlined by dotted lines, and the fields (six pointings) for which J, H, K_s data were taken by SIRIUS are outlined by solid lines.

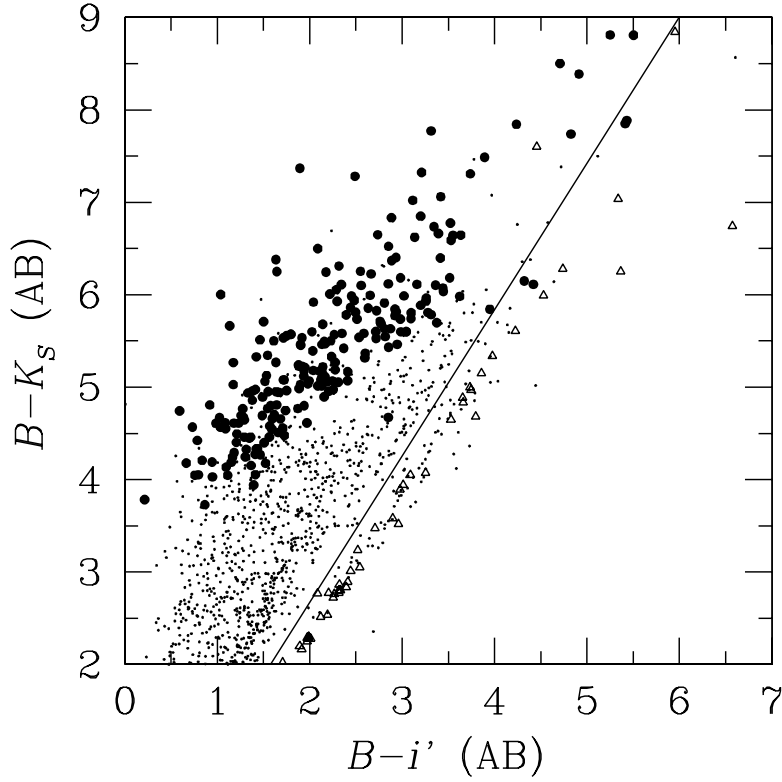


Fig. 2.— Star/galaxy separation using $B - K_s$ and $B - i'$ colors. Objects in the K_s -limited sample are shown by dots and large filled circles. Large filled circles indicate EROs, and triangles correspond to 175 stars given in Gunn & Stryker (1983). The solid line, $B - K_s = 1.583(B - i') - 0.5$, denotes the boundary between stars and galaxies adopted in this study; an object is regarded as a star, if it is located in the right-hand side of this line and its FWHM is $\leq 1.''2$.

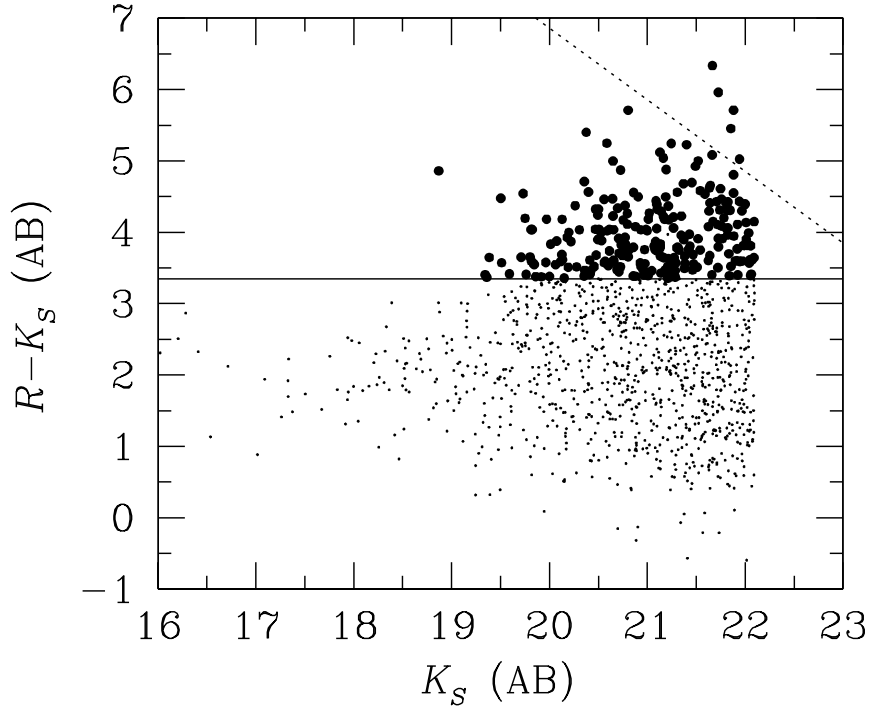


Fig. 3.— $R - K_s$ plotted against K_s for all objects except for stars in the K_s -limited sample. Large circles denote EROs, and the horizontal line corresponds to the threshold ($R - K_s = 3.35$) for selecting EROs. The dotted line indicates the 3σ limiting magnitude of R (26.9).

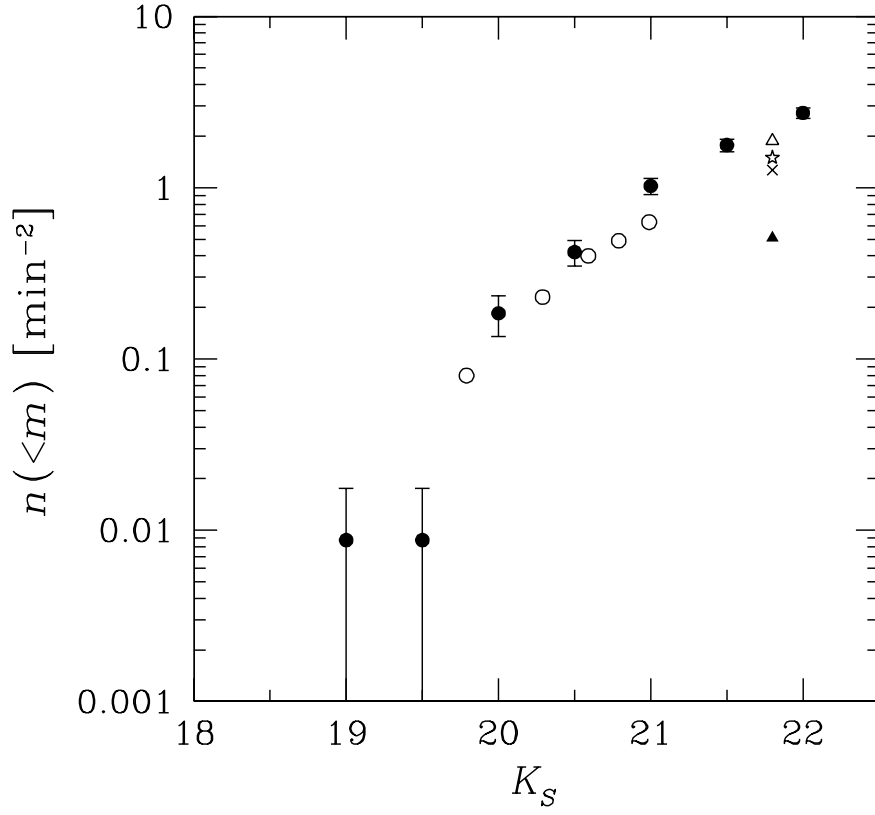


Fig. 4.— Cumulative number counts of EROs. The filled circles denote our results. The data taken from the literature are also shown: Daddi et al. (2000a; based on an area of 701 arcmin²; open circles), Thompson et al. (1999; 154 arcmin²; open triangle), Cimatti et al. (2002; 52 arcmin²; star), Scodeggio & Silva (2000; 43 arcmin²; filled triangle), and Cohen et al. (1999; 14.6 arcmin²; cross), respectively.

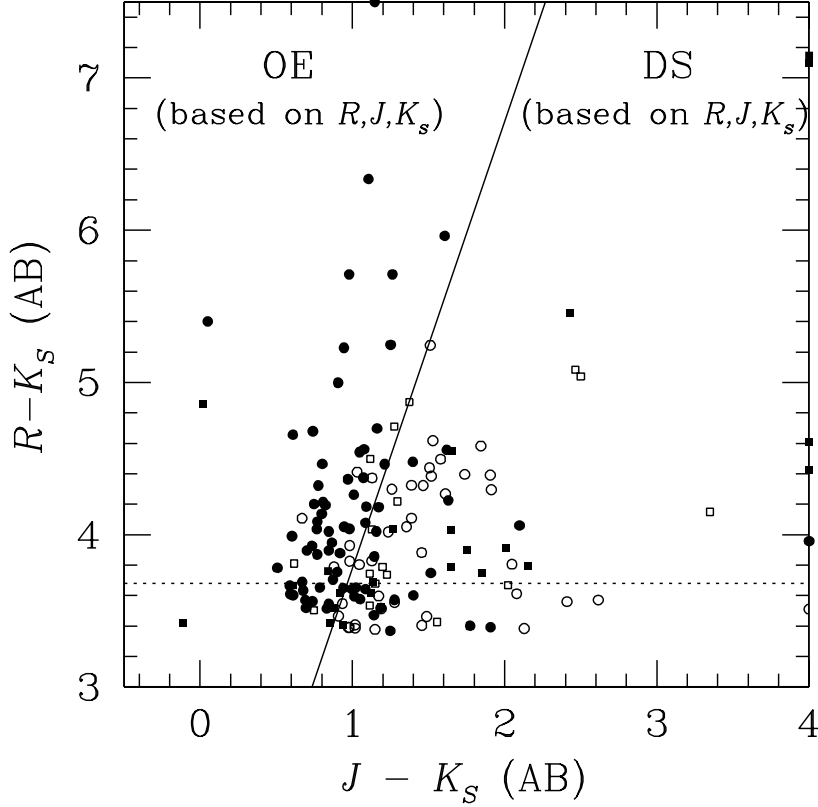


Fig. 5.— $R - K_s$ plotted against $J - K_s$ for EROs in our sample having J magnitude. Filled symbols and open symbols indicate OEs and DSs, respectively, classified by our spectrum fitting method. Objects at $1 \leq z \leq 2$ are shown by circles and those at $z < 1$ or $z > 2$ are shown by squares. Objects with $J - K_s > 3.5$ are plotted on the $J - K_s = 4$ line, and those with $R - K_s > 7.5$ are plotted on the $R - K_s = 7.5$ line. The solid line corresponds to the boundary for separation of OEs and DSs using $R - K_s$ vs $J - K_s$ defined by Mannucci et al. (2002); objects in the right-hand side of this line are classified as DSs. Mannucci et al.’s (2002) classification is valid only for EROs satisfying $R - K_s > 3.68$ (horizontal dotted line) and $1 \leq z \leq 2$. It is expected that our method, which is based on eight bandpasses, gives a better classification over a wider range of redshift.

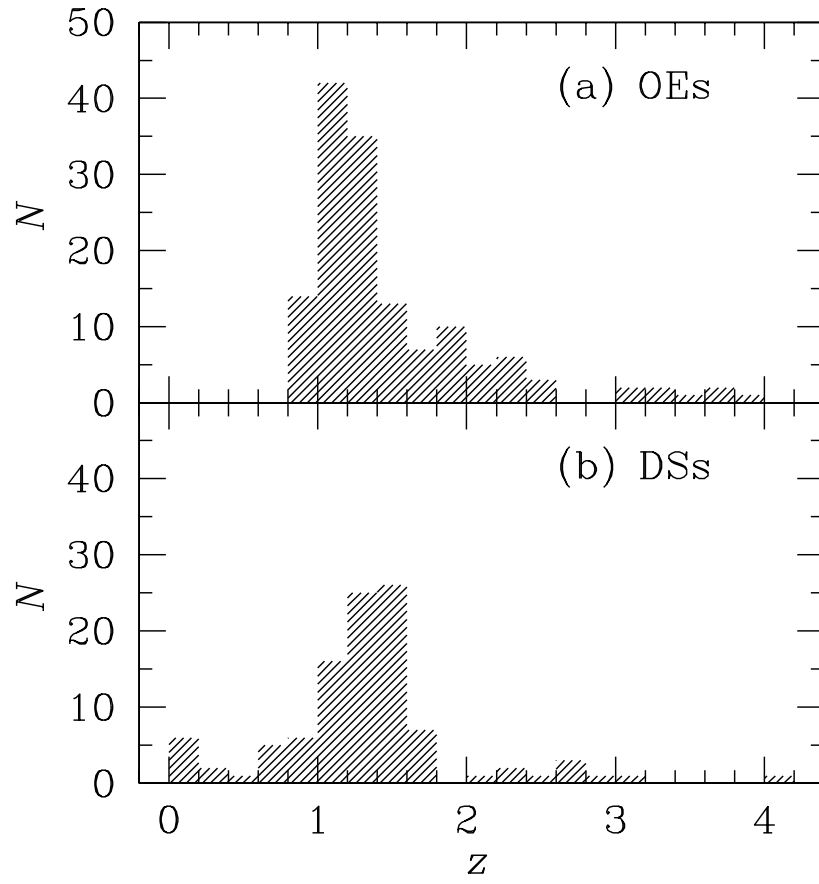


Fig. 6.— Redshift distribution of all EROs in our sample. Panel (a): OEs. Panel (b): DSs.

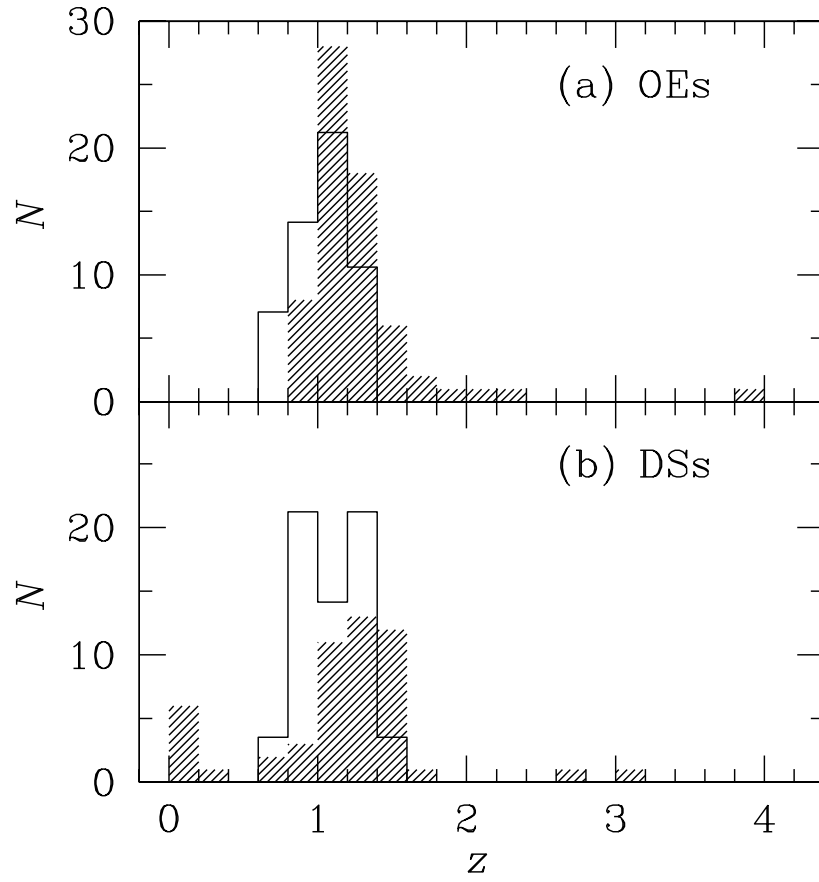


Fig. 7.— Same as Fig. 6, but for EROs with $K_s \leq 21$. The open histograms show the data given in Cimatti et al. (2002; K20 Survey).

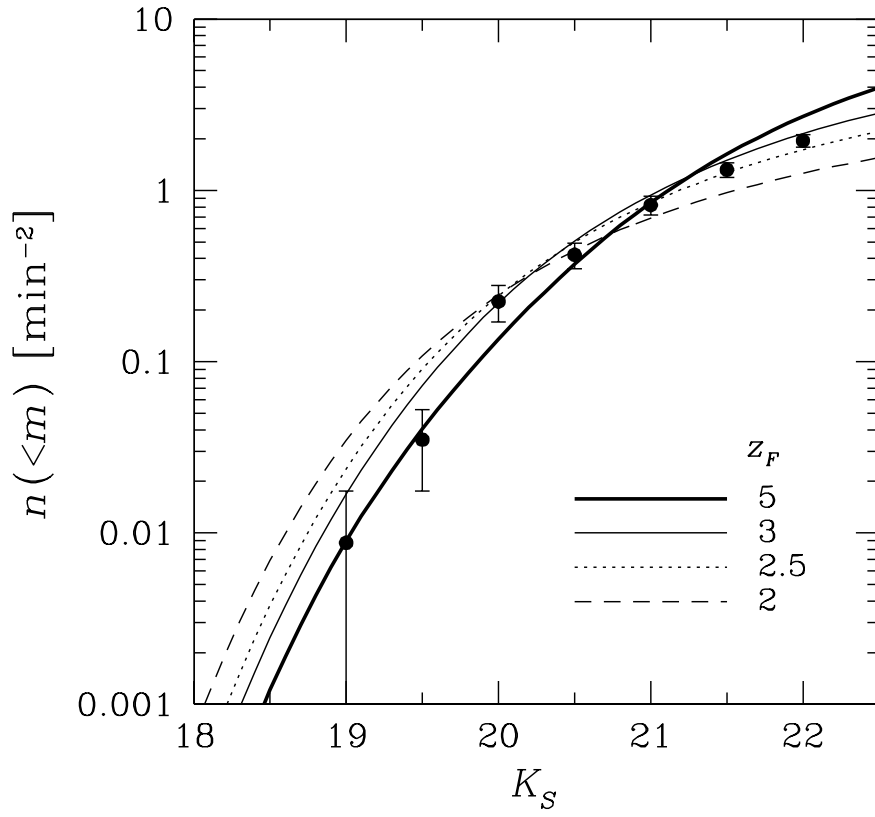


Fig. 8.— Cumulative number counts of OEs in our sample. Predicted counts are plotted by a thick solid line ($z_F = 5$), thin solid line (3), dotted line (2.5), and dashed line (2).

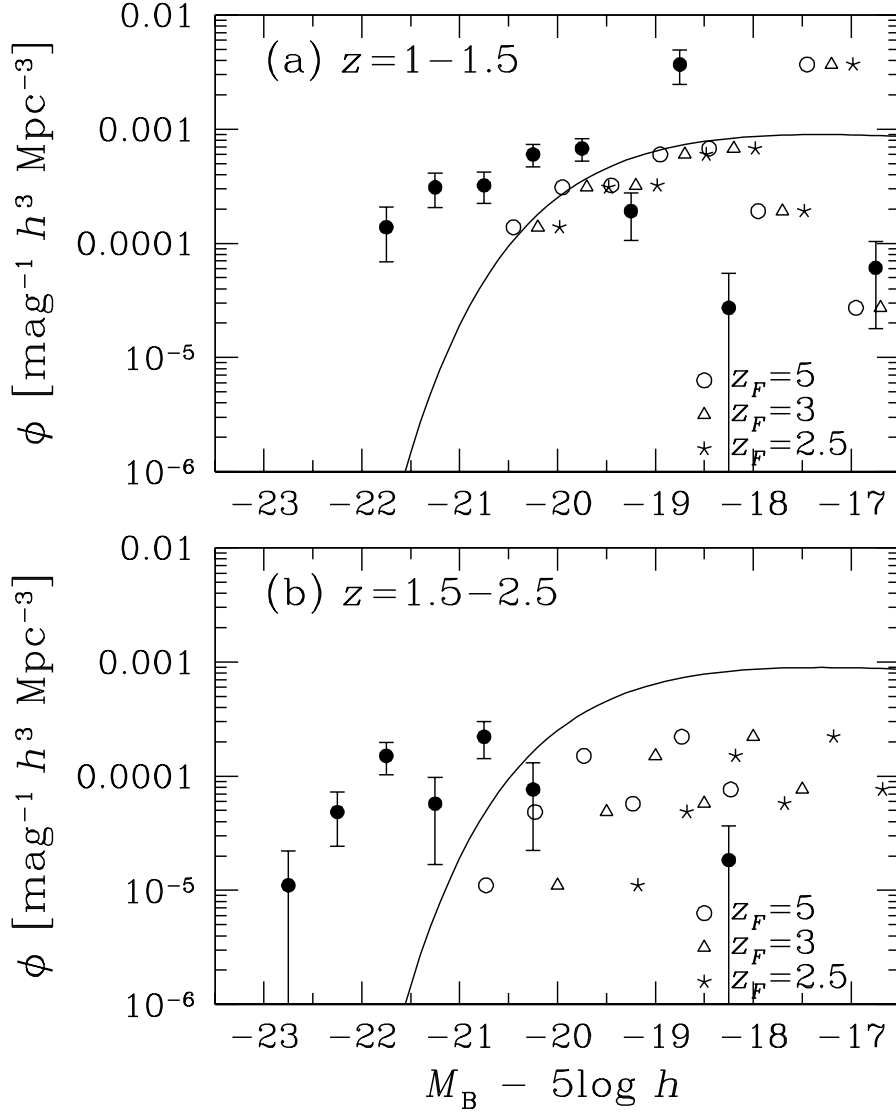


Fig. 9.— Rest-frame B -band luminosity functions (LFs) of OEs (filled circles). Panel (a): objects at $z = 1 - 1.5$. Panel (b): objects at $z = 1.5 - 2.5$. The solid line denotes the local B -band luminosity function for ellipticals given in Marzke et al. (1994). The open circles, open triangles, and stars indicate predictions at $z = 0$ which are calculated by dimming the observed LF to the present on the basis of the passive evolution models with $z_F = 5$, 3 , and 2.5 , respectively, adopted in §5.1.

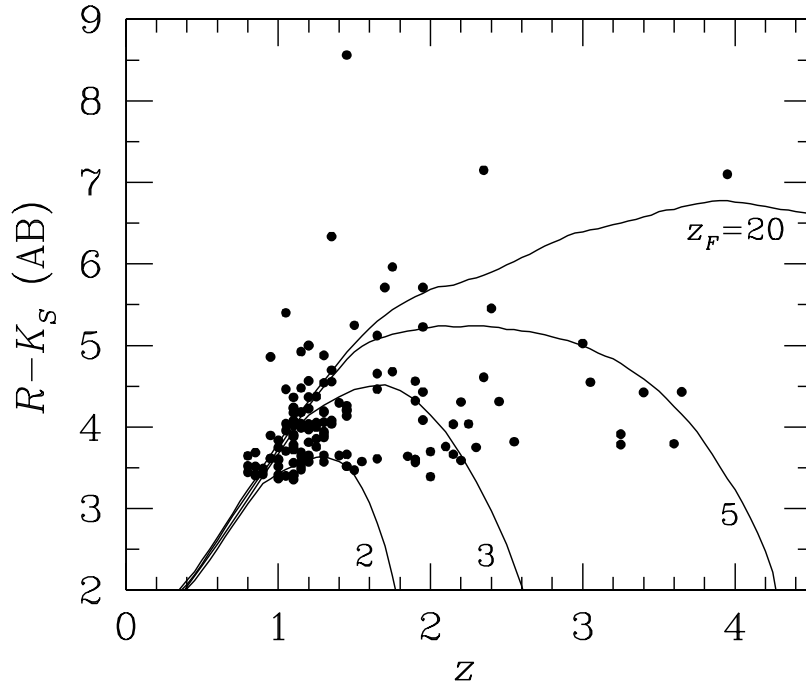


Fig. 10.— $R - K_s$ of OEs plotted against redshift. The four solid lines indicate predictions by passive evolution models with $z_F = 20, 5, 3$, and 2.

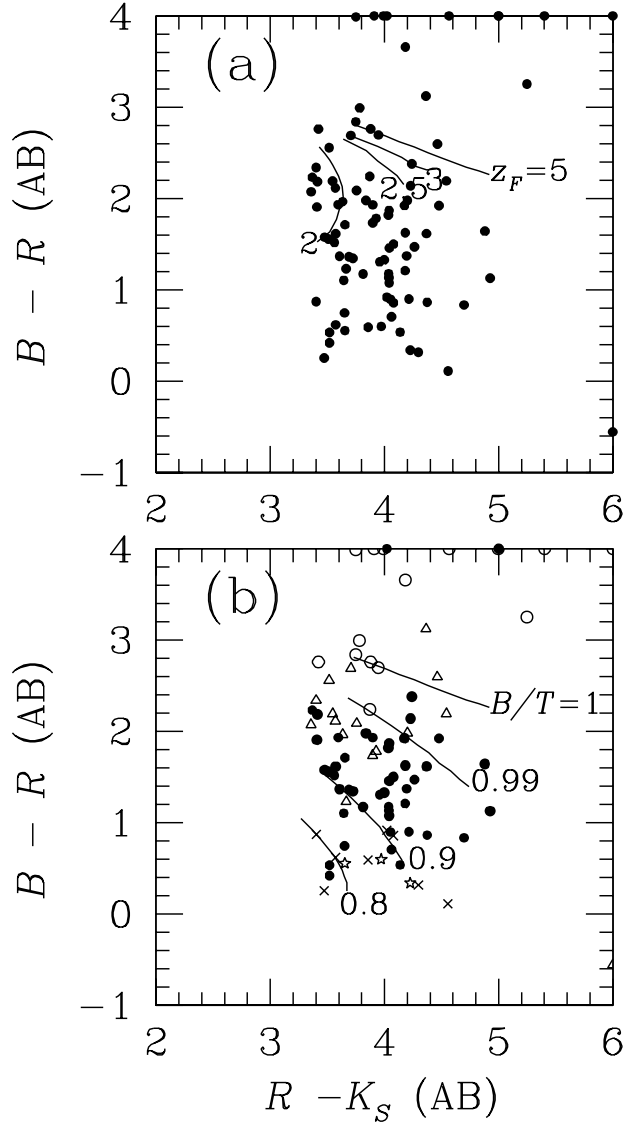


Fig. 11.— $R - K_s$ plotted against $B - R$ for OEs at $z = 1 - 1.5$. Objects with $R - K_s > 6$ are plotted on the $R - K_s = 6$ line, and those with $B - R > 4$ are plotted on the $B - R = 4$ line. Panel (a): Lines show predictions from passive evolution models with $z_F = 5, 3, 2.5$, and 2 . Panel (b): Lines show predictions from bulge plus disk models with $B/T = 1, 0.99, 0.9$, and 0.8 ($z_F = 5$). For the data, different symbols indicate different B/T values; open circles : $B/T = 1$, open triangles : $0.99 \leq B/T < 1$, filled circles : $0.9 \leq B/T < 0.99$, crosses : $0.8 \leq B/T < 0.9$, and stars : $B/T < 0.8$.

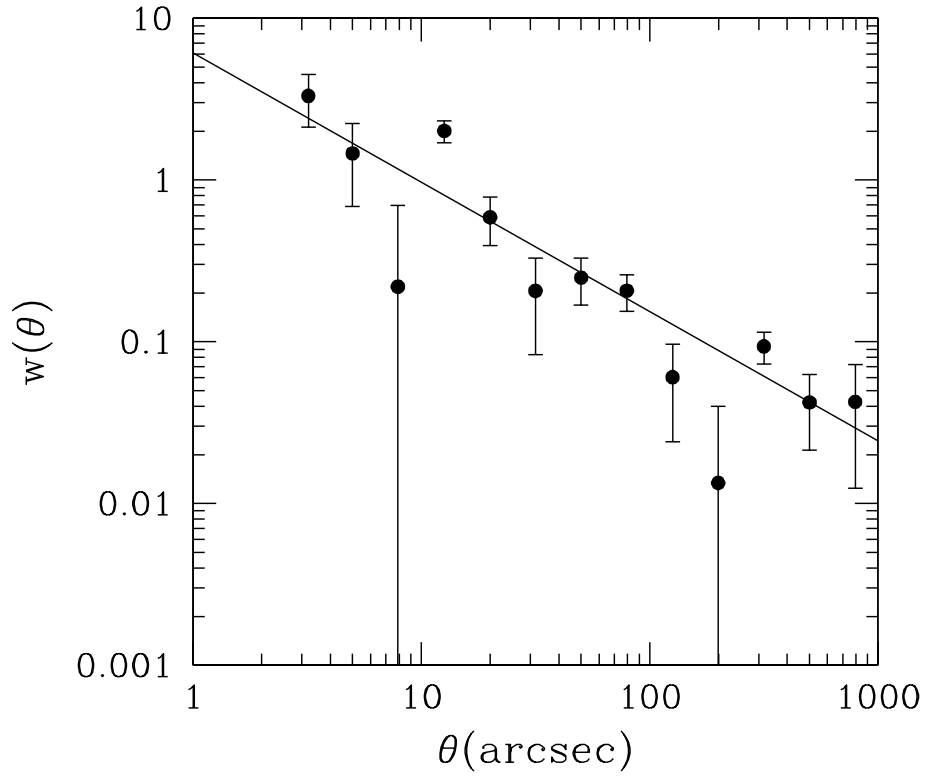


Fig. 12.— Angular correlation function of OEs. The solid line shows the best fit power law with $\omega(\theta) = A_\omega \theta^{-0.8}$ to the data over the range of $3'' \leq \theta \leq 150''$.

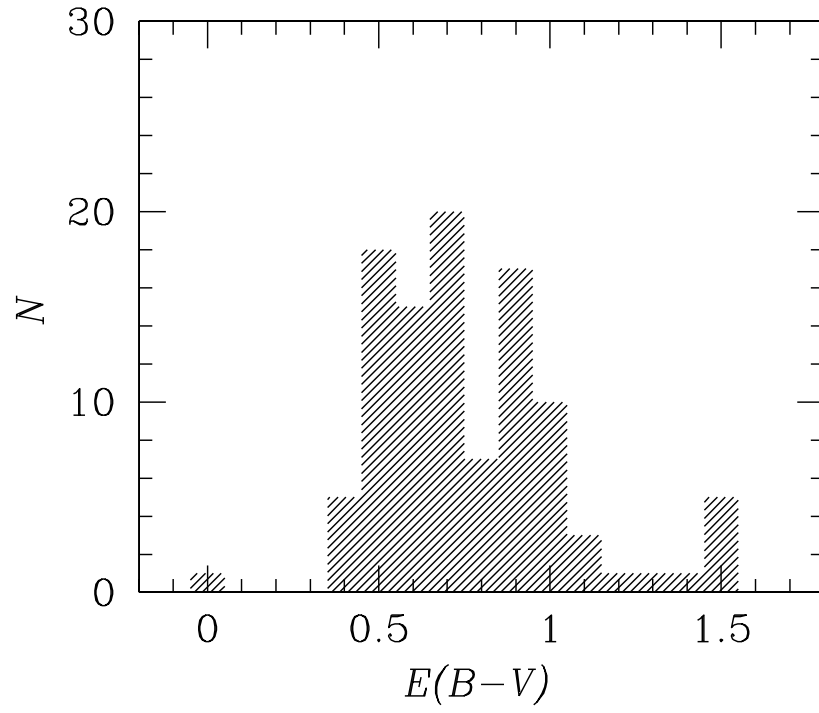


Fig. 13.— Distribution of $E(B - V)$ for DSs in our sample.

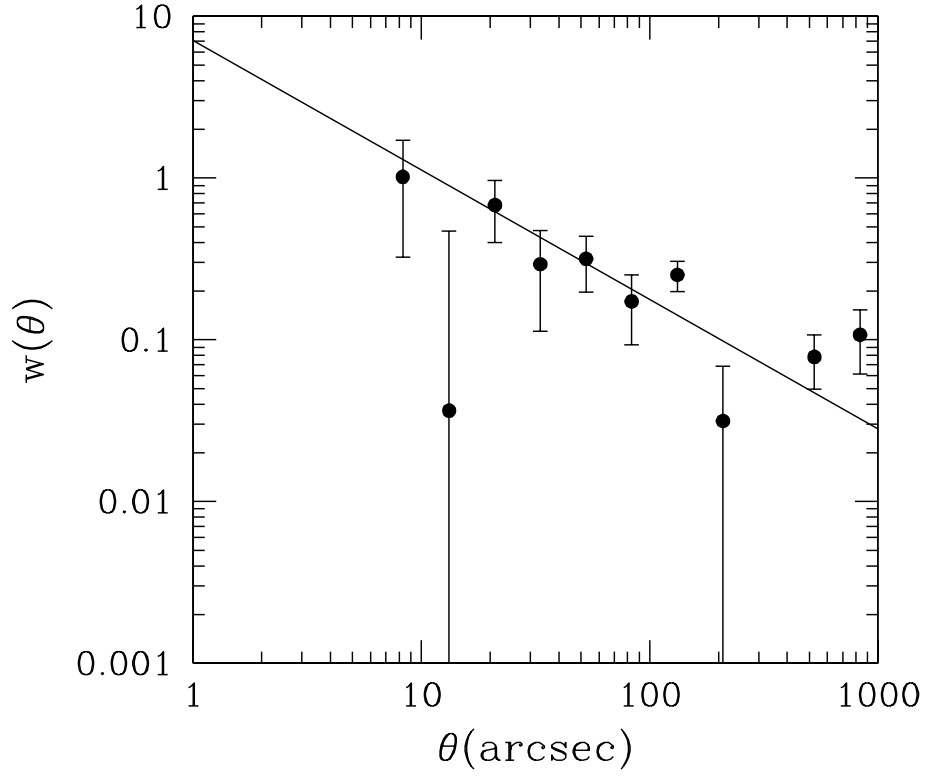


Fig. 14.— Angular correlation function of DSs. The solid line shows the best fit power law with $w(\theta) = A_\omega \theta^{-0.8}$ to the data over the range of $20'' \leq \theta \leq 150''$.

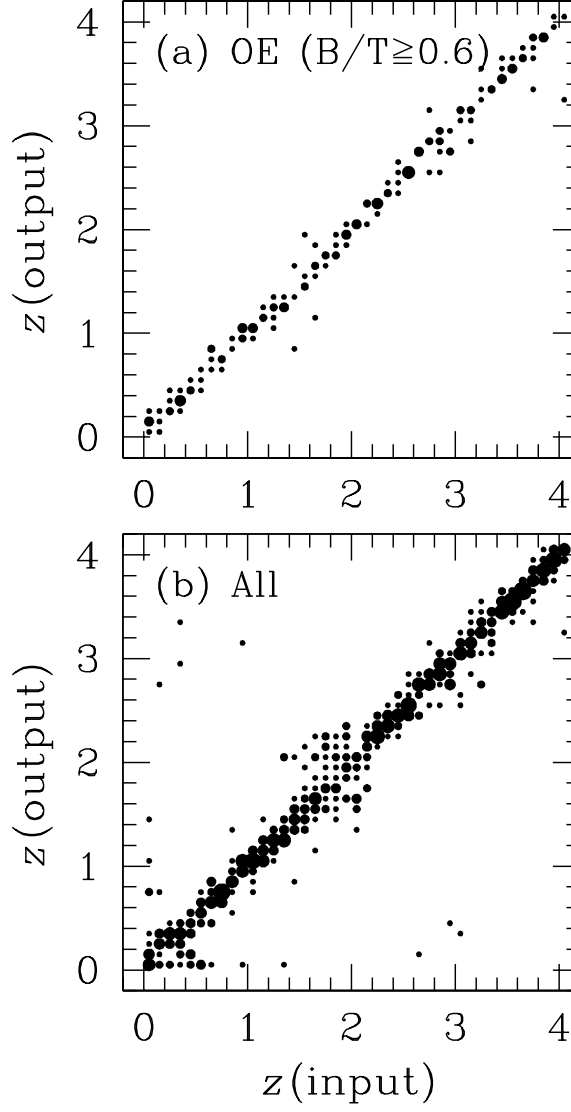


Fig. 15.— Simulations of photometric redshift estimation using model spectra. Abscissa is the redshift of an input spectrum, and ordinate shows the redshift determined from the spectrum fitting to the input spectrum. The area of the filled circles is proportional to the number of objects in the grid. Panel (a): Randomly selected 153 OEs with $B/T(\text{input}) \geq 0.6$. Panel (b): Randomly selected 530 spectra including both OEs and DSs.

Table 1. Summary of the observational data

optical data			
coverage: 618 arcmin ² PSF FWHM: 0''.98			
Band	Exp.[min]	$m_{\text{lim}}^{(a)}$	Obs.Date
<i>B</i>	177	27.1	Nov 2000
<i>V</i>	108	25.9	Nov 2000
<i>R</i>	138	26.3	Nov 2000, Nov 2001
<i>i'</i>	45	25.7	Nov 2000
<i>z'</i>	40	25.0	Oct 2001
infrared data			
coverage: 114 arcmin ² (<i>H</i> , <i>K_s</i>), 77 arcmin ² (<i>J</i>) PSF FWHM: 0''.98			
Band	Exp.[min]	$m_{\text{lim}}^{(a)}$	Obs.Date
<i>J</i>	120	22.8	Aug, Sep 2001
<i>H</i>	120	22.5	Aug, Sep 2001
<i>K_s</i>	120	22.1	Aug, Sep 2001

^(a)5 σ on a 2'' diameter aperture

Table 2. B/T distribution of OEs

B/T	number
0.6	1
0.7	3
0.8	9
0.9	22
0.95	38
0.98	22
0.99	13
0.995	6
0.996	2
0.997	2
0.998	0
0.999	1
1.0	24

Table 3. Parameters of model spectra adopted in this work

SED type	$x^{(a)}$	τ_{SF} [Gyr]	τ_{infall} [Gyr]	t_{GW} [Gyr] ^(b)	Age[Gyr]
OE (pure bulge)	1.10	0.1	0.1	0.2	1.0, 2.0, 3.0, 4.0, 5.0, 6.0, 7.0, 8.0, 9.0, 10.0, 11.0, 12.0, 13.0, 14.0, 15.0
OE (bulge+disk) ^(c)	1.0, 2.0, 3.0, 4.0, 5.0, 6.0, 7.0, 8.0, 9.0, 10.0, 11.0, 12.0, 13.0, 14.0, 15.0
DS	1.35	5.0	5.0	20.0	0.010, 0.013, 0.016, 0.020, 0.025, 0.032, 0.040, 0.050, 0.063, 0.790, 0.100, 0.126, 0.158, 0.200, 0.251, 0.316, 0.398, 0.501, 0.631, 0.794, 1.0, 1.259, 1.585

^(a)Power-law index of initial mass function.

^(b) $t_{\text{GW}} = 20$ means that the galactic wind does not blow until the present epoch.

^(c) $B/T = 0.1, 0.2, 0.3, 0.4, 0.5, 0.6, 0.7, 0.8, 0.9, 0.95, 0.98, 0.99, 0.995, 0.996, 0.997, 0.998, 0.999, 1$, where B and T are the rest-frame bulge and the total luminosity in the B band. The values of x , τ_{SF} , τ_{infall} , and t_{GW} for disks are the same as for DS types.